

EXPERIMENTAL INVESTIGATION OF WAVEFORM TIP INJECTION ON
THE CHARACTERISTICS OF THE TIP VORTEX

A THESIS SUBMITTED TO
THE GRADUATE SCHOOL OF NATURAL AND APPLIED SCIENCES
OF
MIDDLE EAST TECHNICAL UNIVERSITY

BY

YASHAR OSTOVAN

IN PARTIAL FULFILLMENT OF THE REQUIREMENTS
FOR
THE DEGREE OF MASTER OF SCIENCE
IN
AEROSPACE ENGINEERING

SEPTEMBER 2011

Approval of the thesis:

**EXPERIMENTAL INVESTIGATION OF WAVEFORM TIP INJECTION
ON THE CHARACTERISTICS OF THE TIP VORTEX**

submitted by **YASHAR OSTOVAN** in partial fulfillment of the requirements for
the degree of **Master of Science in Aerospace Engineering Department, Middle
East Technical University** by,

Prof. Dr. Canan Özgen
Dean, Graduate School of **Natural and Applied Sciences**

Prof. Dr. Ozan Tekinalp
Head of Department, **Aerospace Engineering**

Asst. Prof. Dr. Oğuz Uzol
Supervisor, **Aerospace Engineering Dept., METU**

Examining Committee Members:

Prof. Dr. Yusuf Ozyoruk
Aerospace Engineering Dept., METU

Asst. Prof. Dr. Oğuz Uzol
Aerospace Engineering Dept., METU

Assoc. Prof. Dr. D. Funda Kurtuluş
Aerospace Engineering Dept., METU

Asst. Prof. Dr. Metin Yavuz
Mechanical Engineering Dept., METU

Prof. Dr. Unver Kaynak
Mechanical Engineering Dept., TOBB-ETU

Date:

I hereby declare that all information in this document has been obtained and presented in accordance with academic rules and ethical conduct. I also declare that, as required by these rules and conduct, I have fully cited and referenced all material and results that are not original to this work.

Name, Last Name: Yashar Ostovan

Signature :

ABSTRACT

EXPERIMENTAL INVESTIGATION OF WAVEFORM TIP INJECTION ON THE CHARACTERISTICS OF THE TIP VORTEX

Ostovan, Yashar

M.Sc., Department of Aerospace Engineering

Supervisor: Asst. Prof. Dr. Oğuz Uzol

September 2011, 62 pages

This study investigates the effect of chordwisely modulated tip injection on the flow and turbulence characteristics of the tip vortex through experimental measurements downstream of a rectangular half-wing that has an aspect ratio of three. This injection technique involves spanwise jets at the tip that are issued from a series of holes along the chord line normal to the freestream flow direction. The injection mass flow rate from each hole is individually controlled using computer driven solenoid valves and therefore the flow injection geometrical pattern at the tip can be adjusted to any desired waveform shape, with any proper injection velocity. The measurements are performed in a blow-down wind tunnel using Constant Temperature Anemometry and Kiel probe traverses as well as Stereoscopic Particle Image Velocimetry. Current data show consistent trends with

previously observed effects of steady uniform tip injection such as the upward and outward motion of the vortex as well as increased levels of turbulence within the vortex core. The vortex size gets bigger with injection and the total pressure levels get reduced significantly near the vortex core. The injection pattern also seems to affect the size of the wing wake as well as the wake entrainment characteristics of the tip vortex. Depending on the injection waveform pattern and injection momentum coefficient the helicoidal shape of the tip vortex also seems to get affected.

Keywords: Tip Vortex, Flow Control, Tip Vortex Control, Tip Injection, Tip Blowing

ÖZ

DALGA ŞEKLİ UÇ ENJEKSİYON YÖNTEMİNİN UÇ GİRDABI KARAKTERİSTİĞİNE ETKİSİ

Ostovan, Yashar

Yüksek Lisans, Havacılık ve Uzay Mühendisliği Bölümü

Tez Yöneticisi : Yard.Doç.Dr. Oğuz Uzol

Eylül 2011, 62 Sayfa

Bu tez çalışmasında veter boyunca modüle edilen uç enjeksiyonu yönteminin kanat uç girdapları üzerindeki etkisi deneysel yöntemler kullanılarak incelenmiştir. Bu teknikte, veter boyunca yerleştirilmiş deliklerden hava akışına dik olacak şekilde, kanat açıklığı boyunca hava enjekte edilmektedir. Enjeksiyon kütle akış oranı her biri ayrı ayrı bilgisayar yardımıyla kontrol edilen solenoid valfler yardımıyla düzenlenmektedir. Bu sayede kanat ucunda üniform veya dalga-şeklinde enjeksiyon senaryoları yaratılabilmektedir. Dört farklı enjeksiyon senaryosu incelenmiştir. Bunlar enjeksiyonsuz ve veter boyunca üniform, üçgen ve sinüs profilli sabit hızlı enjeksiyonlardır. Ölçümler, NACA 0015 profilli ve kanat açıklık oranı üç olan bir yarım kanat geometrisi için, sabit sıcaklıklı sıcak tel anemometresi, Kiel prob taramaları ve Stereoskopik PIV teknikleri kullanılarak kanadın bir veter boyu arkasında elde edilmiştir. Uç enjeksiyonunun, daha önce yapılan çalışmalardaki gözlemlerle de uyumlu olarak, uç girdabını dışarı ve yukarı ittiği, ve uç girdabının çapının da arttığı gözlemlenmiştir. Ayrıca uç enjeksiyonu,

girdap özü içerisindeki toplam basınç kayıplarını ve türbülans yoğunluğunu arttırmaktadır. Ancak bu artış, enjeksiyon momentum katsayısı ile sürekli olarak artmamakta, belli bir momentum katsayısı ve enjeksiyon şekline ulaştıktan sonra düşüş görülmektedir. Enjeksiyon dalga şeklinin de uç girdabı karakteristiklerini önemli ölçüde etkilediği görülmüştür ve uç girdabı etkilerini minimize edecek bir optimum enjeksiyon şeklinin olabileceği düşünülmektedir.

Anahtar Kelimeler: Uç girdabı, akış kontrolü, uç girdabı kontrolü, uç enjeksiyonu, uç üfleme

To my parents,

ACKNOWLEDGMENTS

I would like to express my deep and sincere gratitude to my supervisor Asst. Prof. Dr. Oğuz Uzol. Whose kindness, patience, academic experience and knowledge are invaluable for me at all steps of this thesis study. Without his enthusiasm, energy and support, I could not be able to complete this study.

I would like to thank my jury members Prof. Dr. Unver Kaynak, Assoc. Dr. Funda Kurtuluş, Asst. Prof. Dr. Metin Yavuz and Prof. Dr. Yusuf Ozyoruk for reviewing my thesis.

Lastly, but most importantly, I would like to express my eternal gratitude to my parents for their love, support and encouragement throughout my life.

This study was supported by 108M232 TUBITAK project.

TABLE OF CONTENTS

ABSTRACT.....	iv
ÖZ.....	vi
ACKNOWLEDGMENTS.....	ix
TABLE OF CONTENTS.....	x
LIST OF TABLES.....	xii
LIST OF FIGURES.....	xiii
LIST OF SYMBOLS.....	xvii
CHAPTERS	
1. INTRODUCTION.....	1
1.1 Literature Survey.....	3
1.2 Objectives.....	4
2. EXPERIMENTAL SETUP AND MEASUREMENT DETAILS.....	6
2.1 Flow control wind tunnel.....	6
2.1.1 Wind tunnel and test section design and manufacturing.....	6
2.1.2 Wind tunnel characterization.....	10
2.2 Rectangular wing model and injection system.....	13
2.3 Measurement techniques, Data acquisition and traverse system.....	18
2.3.1 Hot wire single sensor probe and Kiel probe Measurements.....	18
2.3.2 PIV measurements.....	20
2.4 PIV Data Post Processing.....	22

2.4.1	PIV Data Validation	22
2.4.2	Vortex Meandering Effect on PIV Data.....	24
3.	RESULTS.....	27
3.1	Hotwire single sensor and Kiel probe measurement results.....	27
3.1.1	Effect of uniform injection with varying C_μ	27
3.1.2	Effect of injection velocity with constant C_μ	33
3.1.3	Effect of injection waveform with constant C_μ	35
3.1.4	Effect of tip injection with fixed maximum injection velocity (varying waveforms and C_μ).....	41
3.1.5	Effect of tip injection on total pressure loss.....	44
3.2	Stereoscopic PIV measurement results	47
3.3	Energy budget calculations.....	57
4.	CONCLUSION	58
	REFFERNCES	60

LIST OF TABLES

TABLES

Table 3.1 Injection momentum coefficients for each of vortex core locations shown in figure 3.2	31
Table 3.2 Area averaged total pressure minus atmospheric pressure calculations for no injection, triangular injection, quarter-sine injection and uniform injection with a maximum injection velocity of 85 m/s	46
Table 3.3 Injection momentum coefficient, Power consumption and corresponding circulation magnitudes for four injection scenarios.....	57

LIST OF FIGURES

FIGURES

Figure 2.1 – Preliminary design of flow control windtunnel. 3D geometrical view on left and CFD results on right	7
Figure 2.2 – Detailed designed technical sketches of wind tunnel parts: (a) diffuser section, (b) straight section(settling chamber), (c) contraction section.	8
Figure 2.3 – Diffuser, straight section and contraction section detailed designs 3D sketches	9
Figure 2.4 – Wind tunnel 3D sketch and pictures after being manufactured.	9
Figure 2.5 – Transparent test section and model wing 3D sketches and pictures after manufacturing.....	10
Figure 2.6 – Wind tunnel exit velocity for different motor frequency.	11
Figure 2.7– Axial velocity (a), turbulence intensity (b) and total pressure (c) distributions in the wind tunnel contraction section exit (test section inlet). AA’ and BB’ lines are used to extract the distribution of speed along them.....	11
Figure 2.8 – Axial velocity (a), turbulence intensity (b), and total pressure (c) distributions along AA’ and BB’ lines shown in figure 2.7 (a). s parameter indicates the distance in x or y direction	12
Figure 2.9 – Model wing manufactured using rapid prototyping 3D print technique and ten 2.4 mm diameter injection holes distributed uniformly along the chord line.....	13
Figure 2.10 – Ten solenoid valves connected to the wing models injection holes..	14
Figure 2.11 – Pressurized tank 3D model and manufactured one connected to a pressure regulator.....	14
Figure 2.12 – Pulsed Width Modulated signals schematics. T represents corresponding frequency and H is duty cycle	15

Figure 2.13 – Openness ratio for a sample solenoid valve versus duty cycle of the supplying PWM signal.....	16
Figure 2.14 – Injection wave form geometries over wing tip chord.....	16
Figure 2.15 – Injection velocity distribution along the chord at the wing tip for steady uniform injection scenario. Error bars show the standard deviation from the mean at that specific injection hole	18
Figure 2.16 – Kiel probe used in total pressure measurements	19
Figure 2.17 – Schematic of the experimental setup and data-acquisition system for Constant Temperature Anemometry measurements.....	20
Figure 2.18 – Camera settlement schematic for stereo PIV (top left), Left and right cameras located next to test section (top right), Calibration target plate inside the test section (bottom left) and a calibration image captured by left camera (bottom right).....	21
Figure 2.19 – A sample PIV image from one of the cameras visualizing the instantaneous tip vortex for no-injection case (left) and the corresponding instantaneous vector map (right)	22
Figure 2.20 – The 3×3 neighborhood for each vector for the median test.....	23
Figure 2.21 – A sample PIV data before (left) and after (right) median test validation.....	24
Figure 2.22 – Smoke visualization of tip vortex meandering (Roy and Leweke[18])	25
Figure 2.23 – A sample PIV data before and after data processing to remove the vortex meandering effect.....	26
Figure 3.1 – The streamwise velocity magnitude (left), turbulence intensity (middle) and total pressure (right) distributions one chord downstream of the wing. The scenarios are (a) no-injection (b) 50 m/s (c) 60 m/s and (d) 85 m/s uniform injections.....	28
Figure 3.2 – Vortex core approximate locations for this study which is represented in Ostovanetal [19] and Heyes and Smiths’s [9] study. Corresponding injection momentum coefficient for each vortex core location is shown in Table 1.....	31

Figure 3.3 – Turbulence intensity (left) and total pressure (right) distribution one chord downstream of the wing along the horizontal line intersecting the tip vortex core for three different injection scenarios32

Figure 3.4 – The streamwise velocity magnitude (left), turbulence intensity (middle) and total pressure (right) distributions one chord downstream of the wing. (a) 60 m/s uniform (b) 85 m/s uniform (5 hole) injection33

Figure 3.5 – Turbulence intensity (left) and total pressure (right) distribution one chord downstream of the wing along the horizontal line intersecting the approximate tip vortex core for two different injection scenarios 35

Figure 3.6 – Three different injection waveform profiles for 0.075 (right) and 0.1089 (left) injection momentum coefficients36

Figure 3.7 – The streamwise velocity magnitude (left), turbulence intensity (middle) and total pressure (right) distributions one chord downstream of the wing. (a) triangular waveform injection (b) uniform waveform injection (50 m/s) (c) reverse triangular waveform injection.....37

Figure 3.8 – Turbulence intensity (left) and total pressure (right) distribution one chord downstream of the wing along the horizontal line intersecting approximate tip vortex core for each different injection scenarios39

Figure 3.9 – The streamwise velocity magnitude (left), turbulence intensity (middle) and total pressure (right) distributions one chord downstream of the wing. (a) quarter-sine waveform injection (b) uniform injection (60 m/s) (c) reverse quarter-sine waveform injection.....40

Figure 3.10 – Turbulence intensity (left) and total pressure (right) distribution one chord downstream of the wing along the spanwise line intersecting approximate tip vortex core for two different injection scenarios41

Figure 3.11 – The streamwise velocity magnitude (left), turbulence intensity (middle) and total pressure (right) distributions one chord downstream of the wing. (a) no injection (b) steady triangular (c) steady quarter-sine and (d) steady uniform injections. The maximum tip injection velocity for all scenarios is 85 m/s43

Figure 3.12 – Total pressure distributions one chord downstream of the wing. The maximum tip injection velocity for all scenarios is 85 m/s45

Figure 3.13 – Total pressure magnitudes in the approximate vortex center location of each scenario. Corresponding injection momentum coefficient for each scenario is shown on horizontal axis46

Figure 3.14 – Total pressure (left), mean in-plane velocity magnitude with superimposed in-plane streamlines (middle) and the mean vorticity (right) distributions one chord downstream of the wing trailing edge. (a) no-injection (b) triangular injection (c) quarter-sine injection (d) uniform injection50

Figure 3.15 – Mean vortex center locations with respect to the wing ($x/b=0$ is the same as defined in Figure 3.14). The ellipses show the degree of meandering around each vortex center such that the r_x and r_y radii are the root-mean-square values of vortex center position fluctuation around the mean.....51

Figure 3.16 – (a) Mean vorticity and (b) tangential velocity distributions around the mean vortex centers52

Figure 3.17 – Normal stress components' distributions one chord downstream of the wing trailing edge. Black line represents the trailing edge of the wing and the $(x,y)=(0,0)$ coordinate is the corner of the trailing edge and the wing tip54

Figure 3.18 – Shear stress components' distributions one chord downstream of the wing trailing edge. Black line represents the trailing edge of the wing and the $(x,y)=(0,0)$ coordinate is the corner of the trailing edge and the wing tip55

Figure 3.19 – Turbulent kinetic energy and shear stress components distributions around the mean vortex centers for four different injection scenarios56

LIST OF SYMBOLS

A	amplitude of oscillation
b	span
C_{μ}	injection momentum coefficient, $C_{\mu} = \dot{m}_j u_{inj} / q_{\infty} S$
c	chord
h	injection hole diameter
\dot{m}_j	injection mass flow rate
q_{∞}	freestream dynamic pressure
S	wing planform area
u	streamwise wake mean velocity
u_{∞}	streamwise inlet mean velocity
u_{inj}	injection velocity
P_t	wake total pressure
$P_{t\infty}$	inlet air density

CHAPTER 1

INTRODUCTION

Tip vortices are by-products of the lift generated by wings or other lifting surfaces. These vortices have negative effects on wing aerodynamics in general and they can be the cause of a variety of performance and noise related problems in different applications mentioned below:

In transport airplanes because of large span and big wings to produce a large amount of lift force the corresponding tip vortices are enormously big. These vortices lead to various problems for continues take of and landings of airplanes in airports. To avoid tip vortices related problems for transport airplanes in airports the control of tip vortices has become an important issue for researchers in recent years.

In helicopters, vortices produced by rotor blades cause some unsteady changes in pressure distribution for the following blades, and it leads to some dynamic structural problems. On the other hand, blade vortex interaction(BVI) causes noise. Researchers are trying to have less noise and more reliable rotor blades by controlling these tip vortices.

In recent years, particularly by development of miniature electronic technology, Micro Air Vehicles (MAV Micro-Air Vehicles) have been popular. Tip vortices plays an important role in wing aerodynamics of micro air vehicles. The wing spans of these types of aircraft are generally less than 15 cm long, and the aspect ratio is about 1. Because of this property, the tip vortices affects the performance of

the wing with a large impact. So the tip vortex control is critical in the manner of increasing the performance of these types of air vehicles.

Wind turbines, have an important place in the energy sector in recent years due to renewable and clean energy generation. One of the main aerodynamic related problems of wind turbines is tip vortices of blades. Especially in the wind farms the interaction of the tip vortex of one turbine with the turbines in downstream leads to big performance loss. On the other hand, tip vortices are important because of environmental noise pollution caused by wind turbines.

Aircraft gas turbine engines are one of the most affected systems by tip vortices. In these types of engine's turbines and compressors, there is a gap between the rotor blade tips and engine case about 1% to 3% of the blade span which lets the flow to leak from pressure side of the blade to suction side in the tip and generates a tip vortex which dominates the flowfield pressure distribution in that area. This phenomena is called tip leakage, which leads to performance loss of turbine and compressor rotor blades. Generally controlling tip leakage in turbomachines also has an important place to maximize the performance.

The problems in aerospace systems caused by tip vortices mentioned above can be reduced to the minimum by various methods. These methods can be classified to two main parts, passive and active control of tip vortices. Passive methods are generally easy to apply but because of their permanent and fixed effect, they are not efficient for most of the flow conditions. In contrast, active control methods are able to change their effect on the flow field in accordance with flow conditions to have the maximum efficiency. Disadvantage of active control method comparing to passive ones is that active methods are more complicated. Winglets are one of the usual passive control methods for tip vortices. Some of the active vortex control methods examples are: Tip air injection/suction, ejector nuzzles, synthetic jets, electrostatic and plasma methods.

1.1 Literature Survey

Understanding the characteristics of tip vortices and controlling them in an active manner are subjects that have attracted attention in recent years. Some of these studies have focused on understanding the near-field flow structure of a tip vortex to investigate the effect of wing planform shape on tip vortex characteristics (Gerontakos and Lee [1]) and to study the relation between the lift-induced drag, which is computed based on vorticity and the force-balance data (Birch et al [2]). As indicated in Gursul et al [3], lift generation as well as the loading on flight control surfaces could be enhanced while the drag and noise could potentially be reduced by controlling the tip vortex. This can be achieved either by moving a solid surface such as spanwise Gurney flaps [4], active trailing edge flaps [5] and wing tip flaps [6], or by perpendicular or angled tip flow injection, which can be used to modify the strength, location and internal structures of tip vortices (Margaris and Gursul [7]). Bettle [8] investigated the effect of tip injection on the turbulence characteristics of the wake and the tip vortex. It was shown that tip injection causes significant dispersion and outward movement of the vortex as well as excess momentum and increased turbulent kinetic energy within its core. The results of a preliminary experimental investigation on the use of pulsed span-wise jets in the wing tip to perturb a single tip vortex in the very near field are presented by Heyes and Smith [9]. The results demonstrate that the vortex position can be modulated at frequencies up to 50 Hz and, as such, the method shows promise for forcing instability in multiple vortex wakes. Previous studies on tip injection mostly involve steady or uniformly pulsed injection (e.g. Tavella et al. [10], Karthikeyan and Baeder [11, 12], Coton et al. [13]). In addition to these studies that inject a positive mass flow into the main stream, examples of zero-net mass flow rate synthetic jet applications also exist for the control of tip vortices [14, 15].

1.2 Objectives

This study investigates the effect of uniform/waveform steady tip injection on tip vortex characteristics through experimental measurements downstream of a rectangular wing that has an aspect ratio of three. This injection technique involves spanwise jets at the tip that are issued from a series of holes along the chord line normal to the freestream flow direction. The injection mass flow rate from each hole is individually controlled using computer driven solenoid valves and therefore, the flow injection geometrical pattern at the tip can be adjusted to any desired waveform shape, and can be uniform as well as a pre-selected waveform along the chord. The measurements are performed in a blow-down wind tunnel using Stereoscopic Particle Image Velocimetry (PIV), Constant Temperature Anemometry and Kiel probe traverses. Results of various tip injection scenarios, including uniform, triangular, and half-sine waveform injections are presented, and comparisons are made with the baseline no-injection case.

This study is presented in three main parts. Chapter one includes a brief introduction and literature survey about the subject of this study.

Experimental setup and measurement details are presented in chapter two. Wind tunnel design and manufacturing are discussed in this chapter. Constant temperature anemometry, Kiel probe traverses as well as 3D stereoscopic PIV measurement facilities are argued in this section. Data processing and post processing technique details are also described in this chapter.

In chapter 3 measurement results are presented. all measurement are done one chord downstream of the rectangular wing model in an angle of attack of 8 degree. The results of CTA and Kiel probe, as well as PIV and Kiel probe are compared to check consistency.

Chapter 5 includes summary and conclusions as well as the future work that can be done in order to improve the study

CHAPTER 2

EXPERIMENTAL SETUP AND MEASUREMENT DETAILS

In this chapter, experimental setup and measurement details performed in this study, are described in three main parts. The first part talks about the flow control wind tunnel. Second part explains rectangular wing model and injection system and lastly third part contains information about measurement techniques, data acquisition and traverse system.

2.1. Flow control wind tunnel

In this section, the design and manufacturing processes of the wind tunnel are presented, and wind tunnel characterization is discussed.

2.1.1. Wind tunnel and test section design and manufacturing

For experimental investigation of the effects of tip injection on tip vortex characteristics a flow control wind tunnel designed and constructed in the department of aerospace engineering at METU. The preliminary design results are shown in figure 2.1.

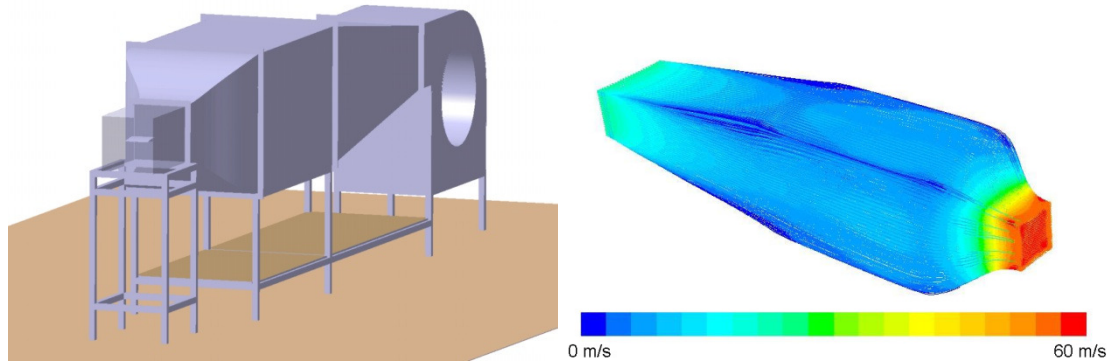
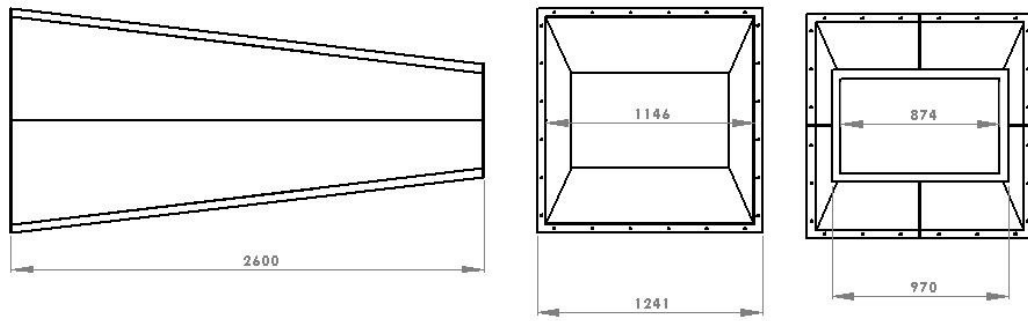
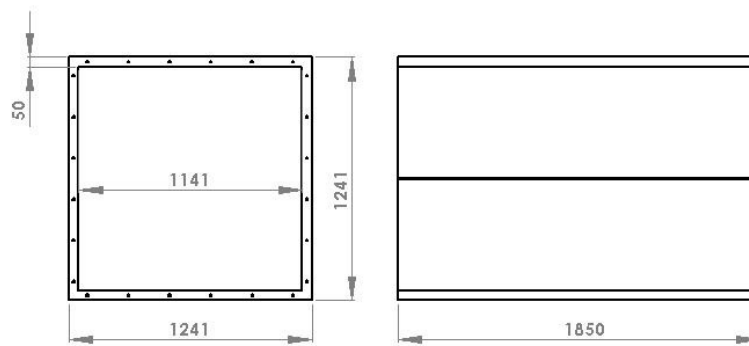


Figure 2.1- Preliminary design of flow control windtunnel. 3D geometrical view on left and CFD results on right

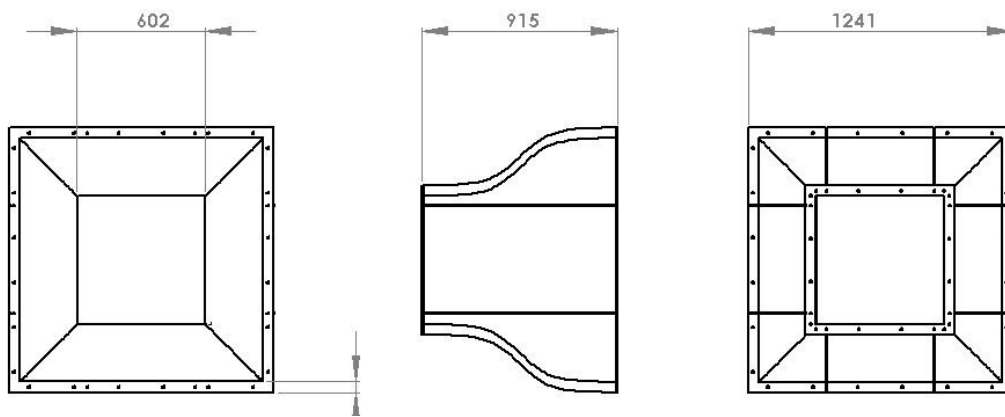
After Preliminary design of wind tunnel each part's detailed design is done using SOLIDWORKS program and technical sketches prepared for manufacturing. Wind tunnel consist of three main parts: diffuser section, straight section (settling chamber), contraction section. Geometrical dimensions of each section is shown in figure 2.2. Diffuser section is 2.6 m long and has a diffusion angle of 7 degree. It has a rectangular cross-section inlet and changes to $1.1 \times 1.1 \text{ m}^2$ square cross-section in outlet (figure 2.2a). There is a radial fan which has a 18.5 KW computer driven AC motor attached to inlet of diffuser. It is a 0.6 m radius double intake radial fan. The outlet of diffuser section is attached to a 1.85 m long straight section with a $1.1 \times 1.1 \text{ m}^2$ square cross section shown in figure 2.2 b. settling chamber is attached to a 0.915 m long contraction with an area ratio of 3.36. The contraction section changes a $1.1 \times 1.1 \text{ m}^2$ cross-section to a $0.6 \times 0.6 \text{ m}^2$ cross section with a tangent hyperbolic contraction profile. Its sketches are shown in figure 2.2 c. 3D models are detailed design for each mentioned part above is shown in figure 2.3. in figure 2.4 the whole wind tunnel model and real manufactured one is pictured. A fully transparent test section is designed and manufactured to be attached to the outlet of windtunnel. It has the capability of holding the model wing in the desired angle of attack. 3D models of test section and manufactured pictures of it are shown in figure 2.5.



(a)



(b)



(c)

Figure 2.2- Detailed designed technical sketches of wind tunnel parts: (a) diffuser section, (b) straight section(settling chamber), (c) contraction section

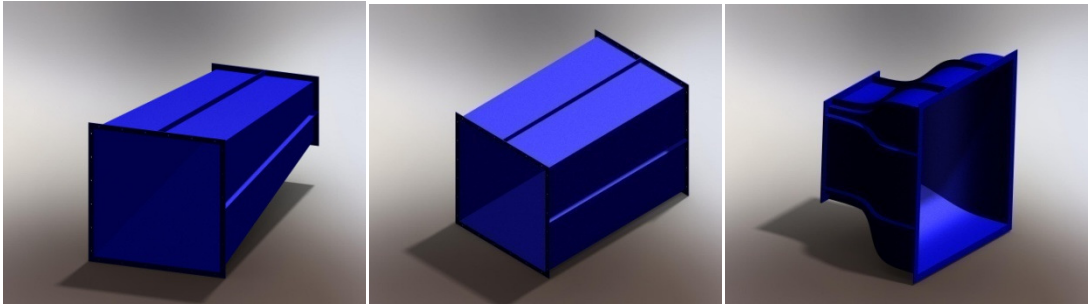


Figure 2.3- Diffuser, straight section and contraction section detailed designs 3D sketches

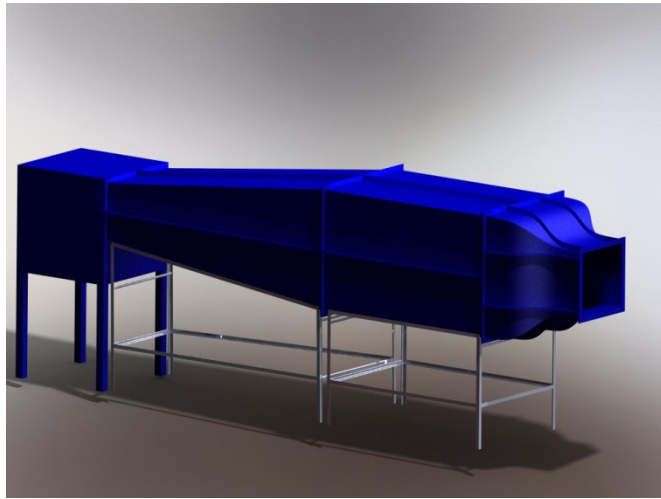


Figure 2.4- Wind tunnel 3D sketch and pictures after being manufactured

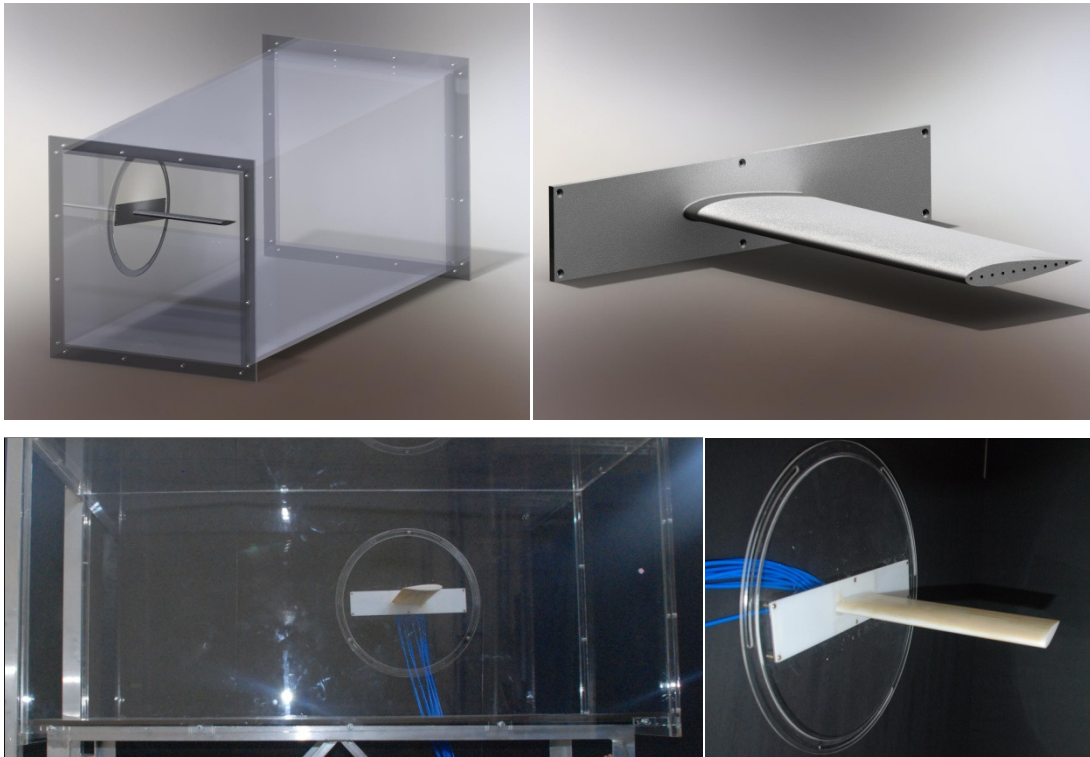


Figure 2.5- Transparent test section and model wing 3D sketches and pictures after manufacturing

2.1.2 Wind tunnel characterization

After wind tunnel construction completion, for different motor speeds of fan the free stream flow velocity is measured in the contraction section outlet. The motor speed can be adjusted by the frequency specified in the motor controller electronic device. Figure 2.6 shows the velocity in contraction section exit versus frequency input for motor controller.

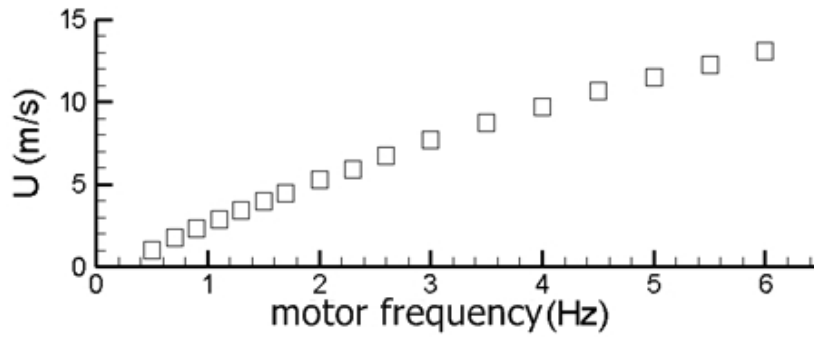


Figure 2.6- Wind tunnel exit velocity for different motor frequency

After wind tunnel fan calibration, For a specified motor speed outlet axial velocity, turbulence intensity and total pressure distributions are measured in contraction exit by traversing a single sensor hot wire probe and a Kiel probe in the plane perpendicular to the flow direction. Figure 2.7 shows the axial velocity, turbulence intensity and total pressure characteristics in the wind tunnel contraction section exit.

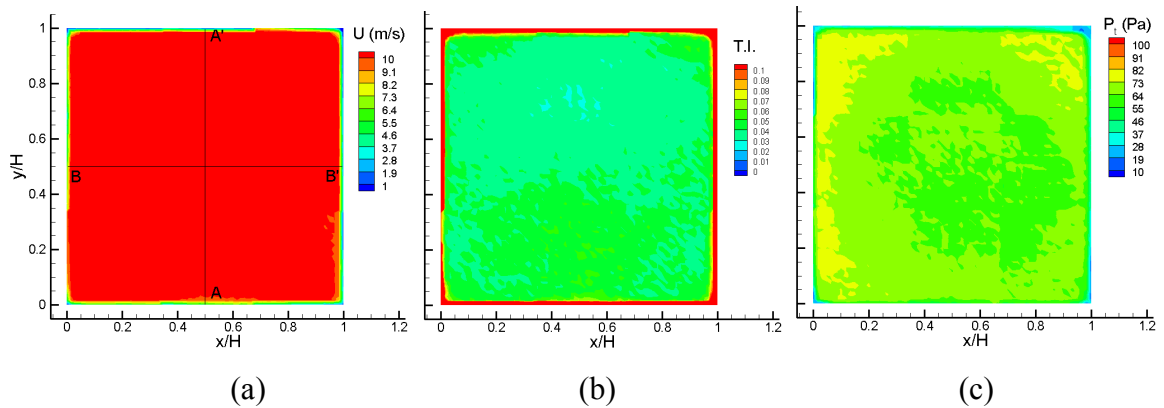


Figure 2.7- Axial velocity (a), turbulence intensity (b) and total pressure (c) distributions in the wind tunnel contraction section exit (test section inlet). AA' and BB' lines are used to extract the distribution of speed along them

The characterization is done for axial velocity of 10 m/s. in figure 2.8 distribution of axial velocity is plotted along AA' and BB' lines shown in figure 2.7 (a).

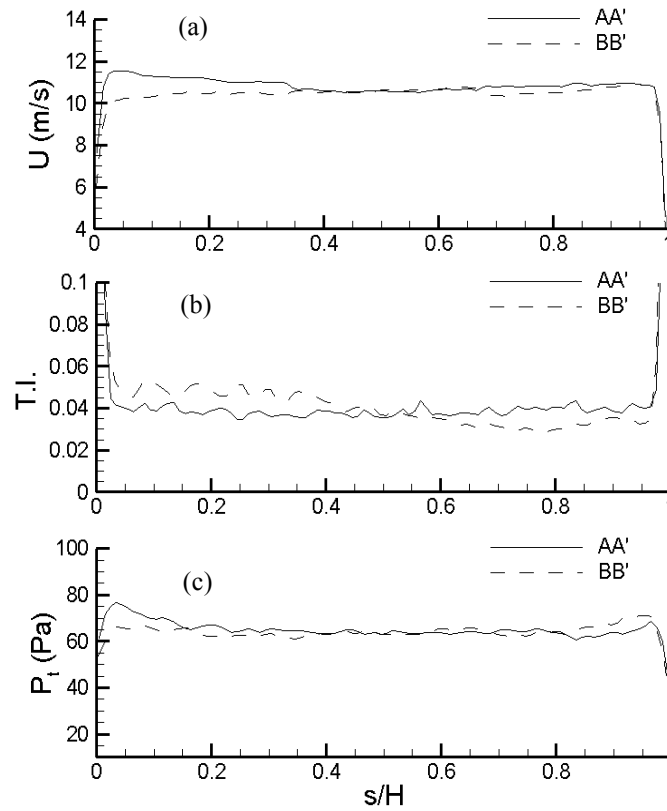


Figure 2.8- Axial velocity (a), turbulence intensity (b), and total pressure (c) distributions along AA' and BB' lines shown in figure 2.7 (a). s parameter indicates the distance in x or y direction

2.2 Rectangular wing model and injection system

The test wing is a 0.1 m chord and a 0.3 m span rectangular wing with a NACA 0015 airfoil profile. This airfoils stall angle is reported to be around 9 degrees for Reynolds number of 75000[22]. The wing can be mounted on the test section sidewall at any desired angle of attack through a rotatable base. . Wing model is manufactured using rapid prototyping 3D print technique. The straight wing tip has ten 2.4 mm diameter injection holes distributed uniformly along the chord line shown in figure 2.9. Each one of these holes is connected to the injection system through independent spanwise flow channels embedded inside the wing. Each injection channel is connected to a dedicated proportional solenoid valve, and all ten valves are connected separately to a common pressurized air chamber outside the tunnel, which supplies the necessary mass flow through the injection channels when the valves are open. Figure 2.10 shows the solenoid valves connected to model wing using 3.2 mm diameter tubes. The chamber pressure is stabilized using two air pressure regulators between the air compressor and the chamber. Figure 2.11 shows the pressurized tank 3D model and manufactured one connected to a pressure regulator.



Figure 2.9- Model wing manufactured using rapid prototyping 3D print technique and ten 2.4 mm diameter injection holes distributed uniformly along the chord line

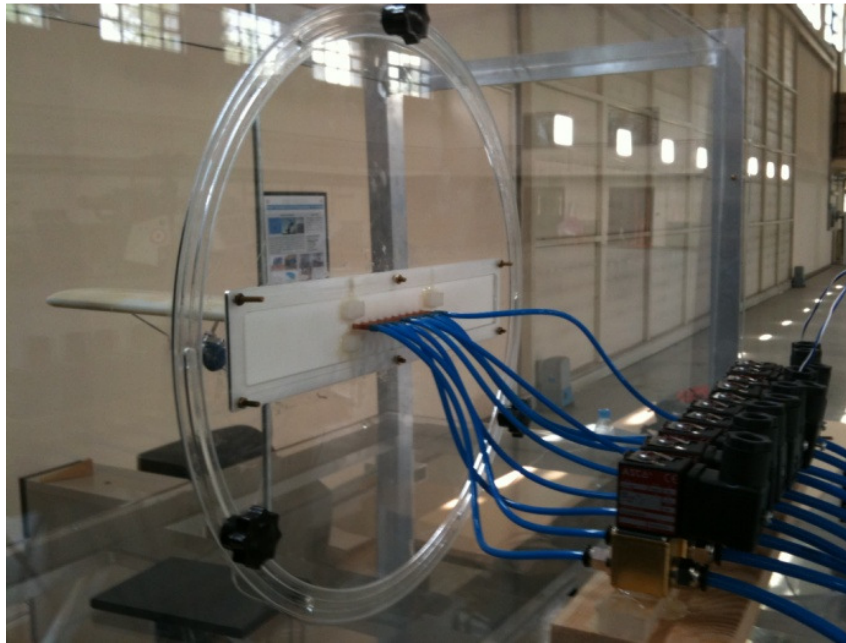


Figure 2.10- Ten solenoid valves connected to the wing models injection holes

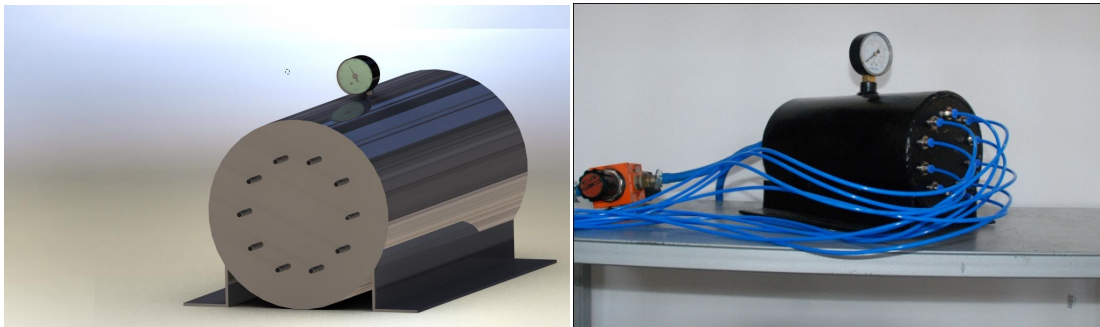


Figure 2.11- Pressurized tank 3D model and manufactured one connected to a pressure regulator

Each one of the solenoid valves is controlled by a Pulse Width Modulated (PWM) signal that is generated by using National Instruments counter signal generator modules (NI PCI 6624 and NI 9472). Figure 2.12 shows schematics of PWM signals. The mass flow rate and therefore, the tip injection velocity from each injection hole is controlled independently by directly changing the duty cycle of the corresponding valve's PWM signal. Figure 2.13 shows the openness ratio for a sample solenoid valve versus duty cycle of the supplying PWM signal. This arrangement allows us to obtain any desired geometrical injection waveform shape along the chord at the wing tip. Figure 2.14 shows the injection waveforms along the wing model chord used in this study.

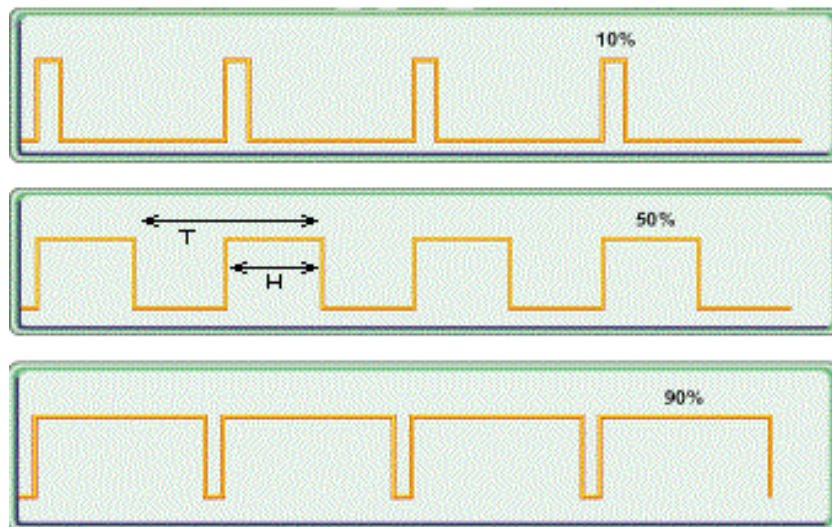


Figure 2.12- Pulsed Width Modulated signals schematics. T represents corresponding frequency and H is duty cycle

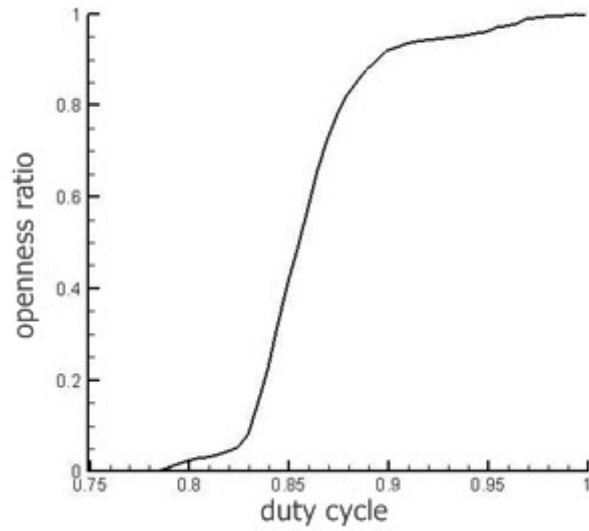


Figure 2.13- Openness ratio for a sample solenoid valve versus duty cycle of the supplying PWM signal

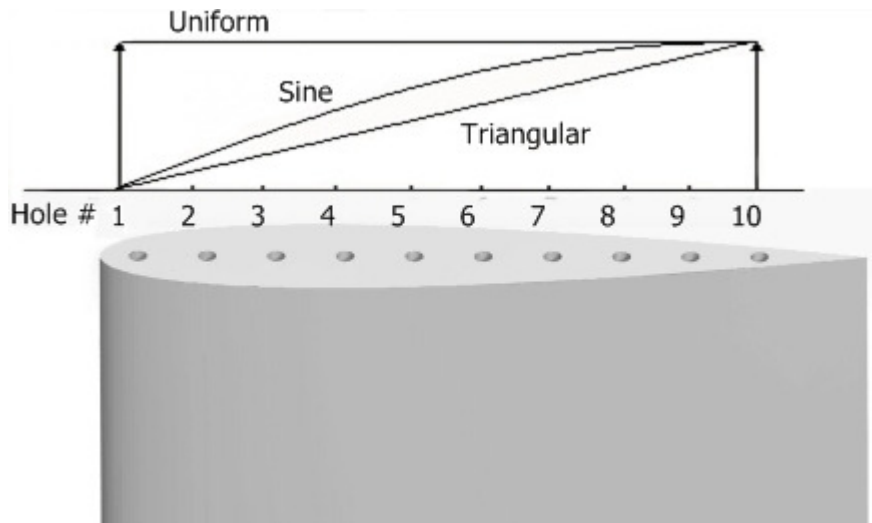


Figure 2.14- Injection wave form geometries over wing tip chord

The rate of blowing is characterized by injection momentum coefficient as defined below. In this definition \dot{m}_j represents mass injection rate, u_{inj} is the injection velocity, q_∞ is the free stream dynamic pressure and S is the area of the wing. C_μ is calculated for each hole separately and added up to get the total injection momentum coefficient.

$$C_\mu = \dot{m}_j u_{inj} / q_\infty S$$

In order to check the variations in the injection velocity during the data acquisition period, the tip injection velocity is measured in front of the each injection hole for a 15-minute time interval using Kiel probe measuring total pressure in each hole exit. The velocity is calculated from total pressure using Bernoulli equation. In this calculation, the static pressure is assumed to be equal to atmospheric static pressure, and density is assumed to be constant. The mean injection velocity distribution along the chord and the standard deviation values for each hole are calculated for the uniform steady injection case, and the results are presented in Figure 2.15. As can be seen from the figure, the mean injection velocity is about 84.8 m/s, which corresponds to an injection momentum coefficient C_μ of 0.2179, with a maximum standard deviation of 0.669 m/s.

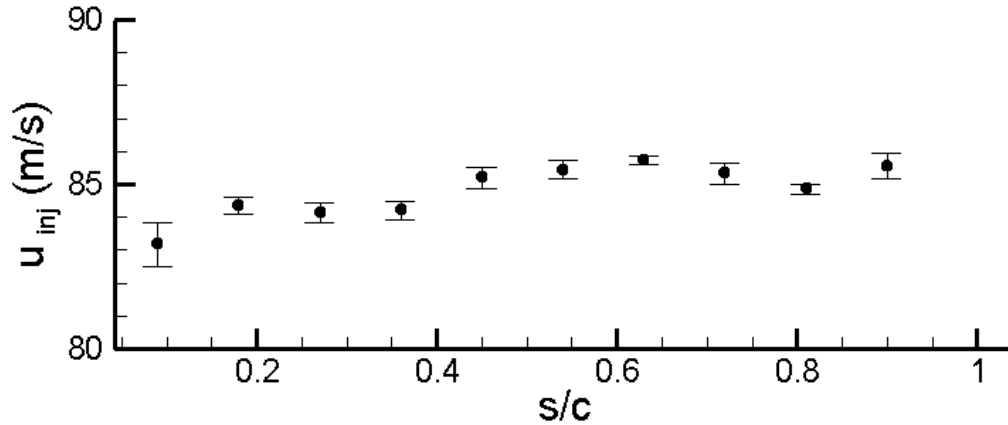


Figure 2.15- Injection velocity distribution along the chord at the wing tip for steady uniform injection scenario. Error bars show the standard deviation from the mean at that specific injection hole

2.3 Measurement Techniques, Data Acquisition And Traverse Systems

This section presents details of measurement techniques conducted in this study. Specifications of the devices used are also discussed briefly.

2.3.1 Single Sensor Hotwire And Kiel Probe Measurements

All measurements are performed at a free-stream velocity of 10 m/s and at an angle of attack of 8 degrees. The corresponding Reynolds number is about 67000 based on the chord of the wing. Single sensor hot-wire and Kiel probe traverses are conducted one chord downstream of the wing scanning a $0.1325 \times 0.12 \text{ m}^2$ area with 2.5 mm resolution, which generated 2646 measurement points in total. At each measurement point data is sampled at 5 kHz for 2 seconds using the data-acquisition system. The

velocity and turbulence data are obtained using a single sensor hot-wire probe driven by a DANTEC 54N81 multi-channel CTA module. The data acquisition from the hot-wire module is obtained using a NI 9205 analog input module with a maximum capacity of 250 kS/s aggregate sampling rate. As the constant temperature anemometry measurement sensor is highly sensitive to temperature changes. Before each hot wire measurement hot wire system should be calibrated using a reference probe. Total pressure data is obtained using a 3.175 mm shield diameter Kiel probe and a Scanivalve DSA3217 pressure module. Pictures of Kiel Probe are shown in figure 2.16. The tip flow injection, probe traverse and data-acquisition systems are all controlled using LABVIEW software through a personal computer. Figure 2.17 shows a schematic of the experimental setup and data-acquisition system for Constant Temperature Anemometry measurements.



Figure 2.16- Kiel probe used in total pressure measurements

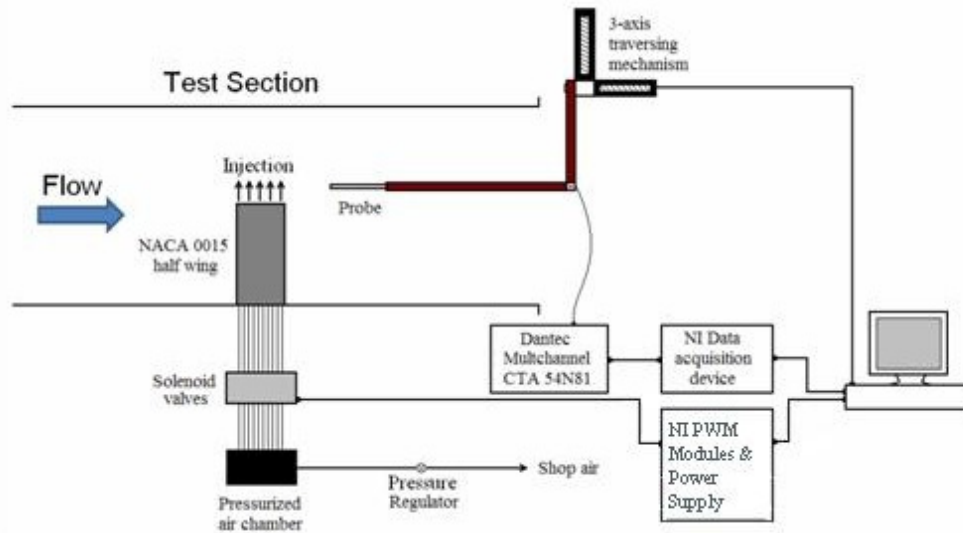


Figure 2.17- Schematic of the experimental setup and data-acquisition system for Constant Temperature Anemometry measurements

2.3.2 PIV Measurements

Stereoscopic PIV measurements are performed one chord downstream from the wing trailing edge using a 120 mJ/pulse 532 nm Nd:YAG laser for illumination and two 1344x1024 12-bit resolution HiSense Mk II CCD cameras each equipped with a 60 mm Nikon Mikro Nikkor lens. Figure 2.18 shows PIV setup and the data measurement plane. A commercial fog generator is used for seeding the flow. Calibration for stereoscopic measurements is done by moving target plate two steps downstream and two steps upstream of the measurement plane in flow direction to capture calibration images in each step. The distance between calibration images' plane is 1mm. Bottom left image in figure 2.18 shows the target plate attached to the traverse system placed in test section in order to obtain calibration images.

The synchronization of the laser and the cameras is performed using the Dantec Flow Manager hub and the Dantec Flow Manager software is used to collect and process the images. Calibration is performed by traversing a 200 mm x 200 mm target plate. Adaptive correlation is performed to get the vector maps from images. The final interrogation area size is 32 pixels (vertical and horizontal). The size of overlap is 50%. 3D vector maps are obtained using two 2 vector maps from images captured by right and left cameras. For 3D vector analysis over sampling factors are 1 for X and Y directions. A sample PIV image and corresponding vector map is shown in figure 2.19.

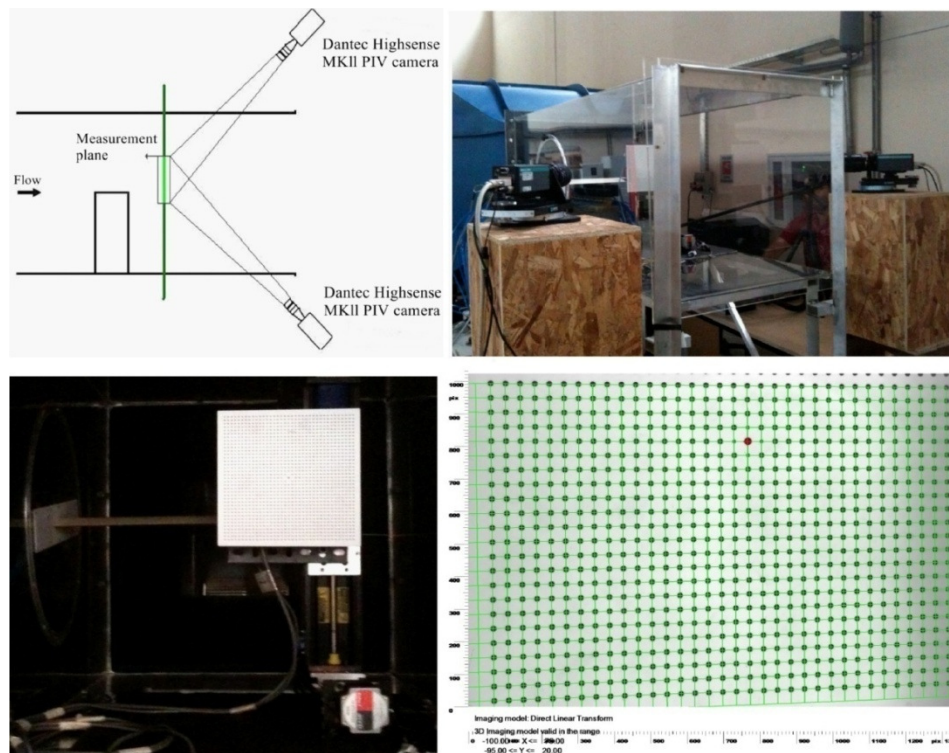


Figure 2.18- Camera settlement schematic for stereo PIV (top left), Left and right cameras located next to test section (top right), Calibration target plate inside the test section (bottom left) and a calibration image captured by left camera (bottom right)

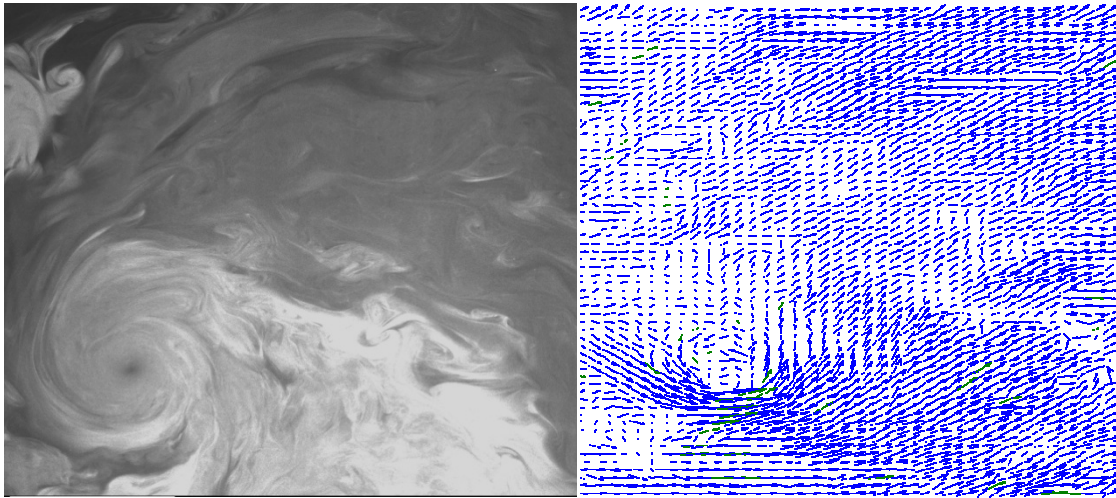


Figure 2.19- A sample PIV image from one of the cameras visualizing the instantaneous tip vortex for no-injection case (left) and the corresponding instantaneous vector map (right)

2.4. PIV Data Post Processing

PIV data needs to be post processed. This process consists of two main parts as follows: PIV data validation and subtracting the meandering effect from data.

2.4.1 PIV Data Validation

The Raw PIV instantaneous vector maps obtained from Dantec software are further examined, and unacceptable maps are manually rejected by eye detection. For each measurement case, 600 raw vector maps are obtained and Approximately, 17% are rejected in this stage. Then the median test algorithm described in [16] is applied to filter the vector maps. The median test is performed in the 3×3 neighborhood for each vector. A schematic of mentioned neighborhood is shown in figure 2.20. Firstly,

median of eight vectors in the neighborhood is computed denoted by U_m . Then for each of those eight vectors a residual r_i , $r_i = |U_i - U_m|$ is calculated. r_m is the median for r_i , $i=1, \dots, 8$. In the equation shown below U_0 represents the examined vector, and ϵ is a constant to guarantee a minimum normalization level.

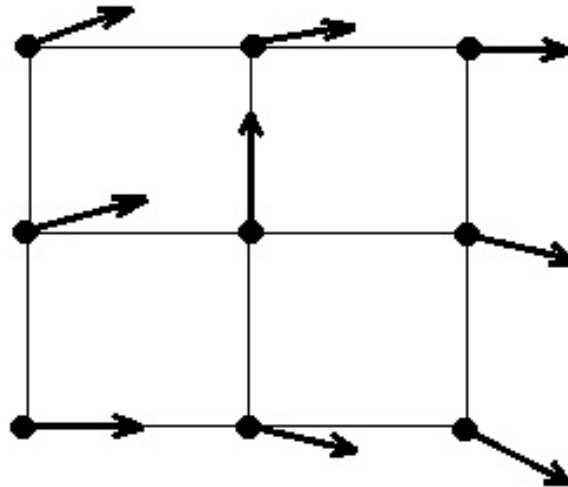


Figure 2.20- The 3×3 neighborhood for each vector for the median test

$$r_0^* = \frac{|U_0 - U_m|}{r_m + \epsilon}$$

If the normalized fluctuation level is more than specified magnitude, the vector is replaced by the median value of the neighborhood vectors U_m . The median test filtering is done using a code written in FORTRAN program. Figure 2.21 shows a sample PIV data before and after median test validation.

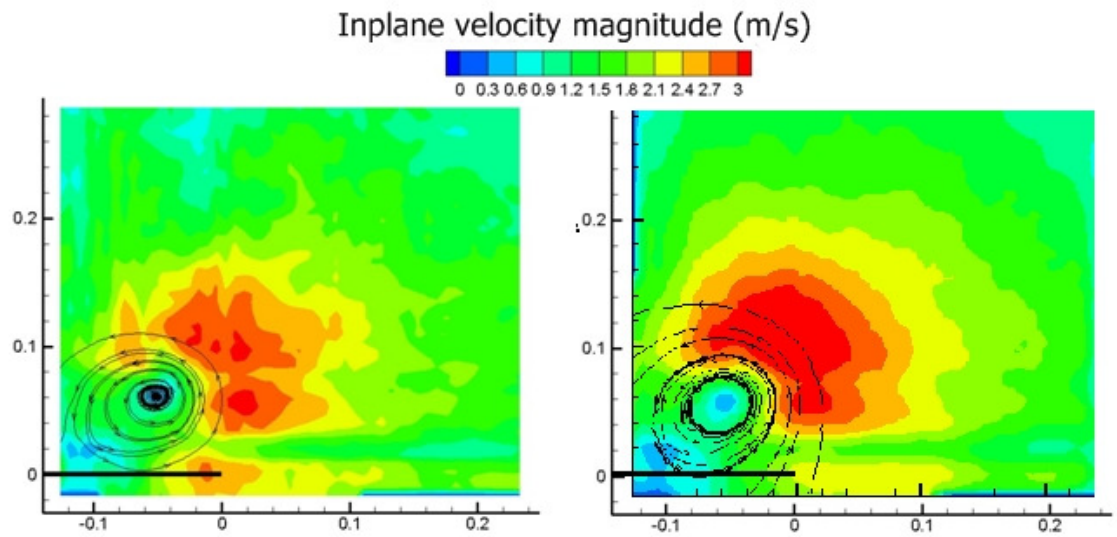


Figure 2.21- A sample PIV data before (left) and after (right) median test validation

2.4.2 Vortex Meandering Effect on PIV Data

Vortex meandering represents the fast and unstable displacements of the vortices studied in tip vortex measurements experiments. It is a repetitive feature which is almost the main source of uncertainties in point measurements of vortices in wind tunnels for PIV measurement technique [16]. Figure 2.22 shows a tip vortex meandering smoke visualization. Before calculating the average flow fields, the vector maps are processed to remove vortex meandering effects using the methodology described in [17]. On each instantaneous vector map data, vortex centers are identified using the maximum vorticity location. This location is recorded and necessary coordinate shifts are performed to re-center the vector maps such that the instantaneous vortex centers will be at $(x,y)=(0,0)$ coordinate. Because of this shift in

coordinates for each instantaneous dataset, common overlap regions are determined for each injection scenario, which are then used for the calculation of the ensemble average flow fields. In the current study, we used 140 vector maps for averaging after the removal of the vortex meandering effects. Recorded meandering data are also used to quantify the amount of vortex meandering in each case. Figure 2.23 shows a sample PIV data before and after removing the vortex meandering effect.



Figure 2.22- Smoke visualization of tip vortex meandering (Roy and Leweke[18])

One of the most important points to note here is that the tip vortex meandering reduces the area of observation. Another issue is that equivalent speed magnitude bands on the plot have changed from oval shape to be circular. So, their oval shape can be considered as an effect of vortex meandering.

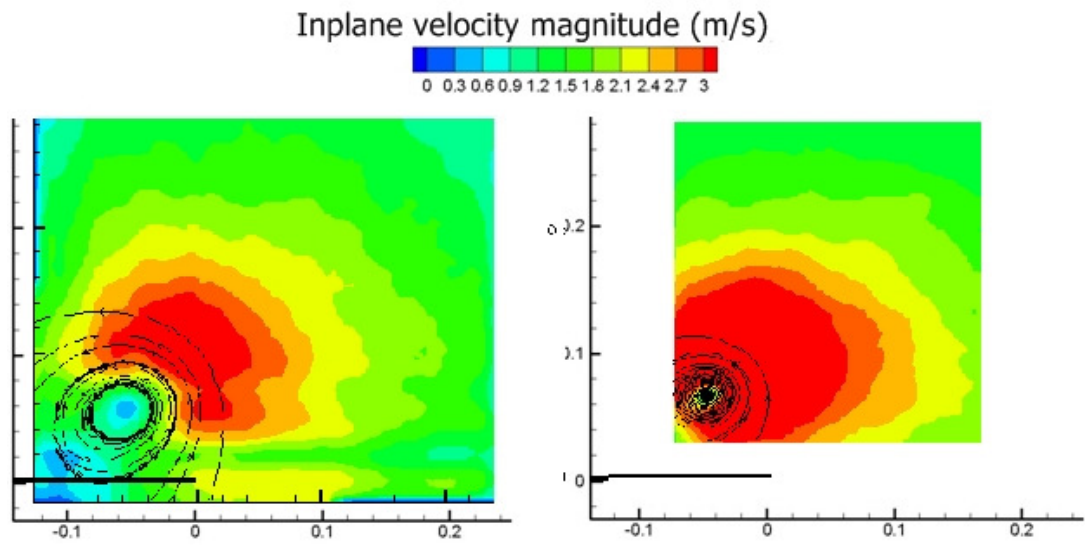


Figure 2.23- A sample PIV data before and after data processing to remove the vortex meandering effect

CHAPTER 3

RESULTS

In this chapter, the results of single sensor hotwire measurements, Kiel probe measurements and Stereoscopic PIV measurements are presented, compared and discussed.

3.1. Single Sensor Hotwire and Kiel Probe Measurement Results

In this section, single sensor hotwire and Kiel probe measurements are presented and discussed. Firstly, the effect of uniform injection with varying C_μ is presented, then the Effect of injection velocity with constant C_μ is studied. After, Effect of the injection waveform with constant C_μ is discussed and finally, Effect of tip injection with fixed maximum injection velocity (varying waveforms and C_μ) is presented.

3.1.1. Effect of uniform injection with varying C_μ

In this section, hot wire and Kiel probe measurement results for uniform injection with three different injection momentum coefficients are presented and compared to no injection case. Three of the scenarios involve a steady chord wisely uniform injection from the tip with different injection velocities, i.e. 50 m/s, 60 m/s and 85 m/s. The

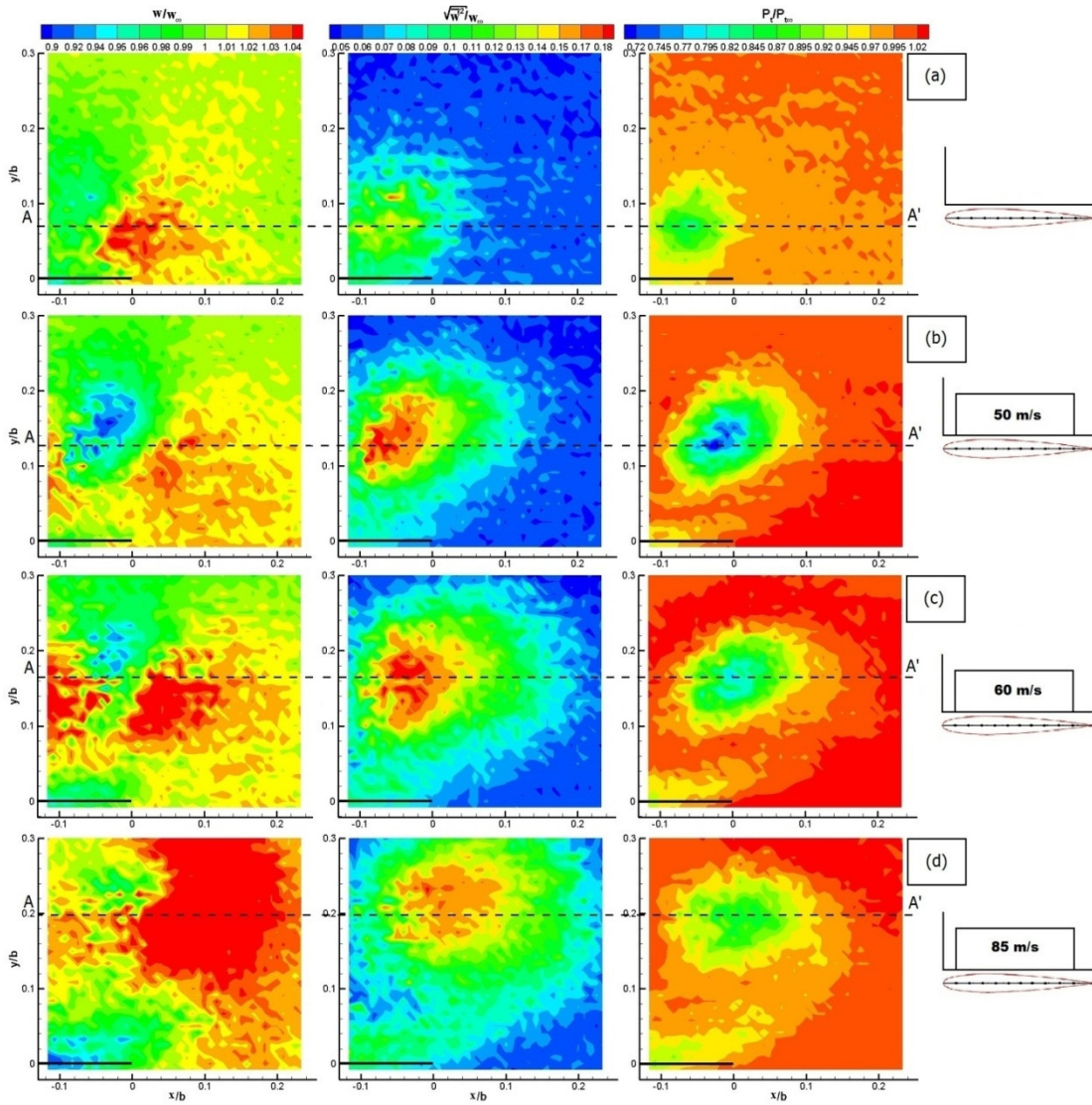


Figure 3.1- The streamwise velocity magnitude (left), turbulence intensity (middle) and total pressure (right) distributions one chord downstream of the wing. The scenarios are (a) no-injection (b) 50 m/s (c) 60 m/s and (d) 85 m/s uniform injections

injection momentum coefficients, C_{μ} , for each of the scenarios are 0.0767, 0.1089 and 0.2179 for 50 m/s, 60 m/s and 85 m/s injection speeds, respectively. The results are compared to the case with no injection from the wing tip.

Figures 3.1a, b, c and d present the distributions of streamwise velocity magnitude and turbulence intensity as well as total pressure one chord downstream of the wing for no injection, uniform 50 m/s, 60 m/s and 85 m/s chord wisely uniform injection scenarios, respectively. The black lines in these figures designate the location of the trailing edge of the wing and the (0,0) coordinate is at the trailing edge of the tip of the wing. The main flow direction is coming out of the page (i.e. we are facing upstream direction) and all coordinates are non-dimensionalized by the span, b .

For all injection scenarios, a well-defined tip vortex can be depicted in general by localized regions of elevated total pressure loss and increased levels of turbulence intensity. The wake of the wing is also visible as a low total pressure and high turbulence zone. In the case of no-injection (Figure 3.1 a), the diameter of the vortex is about 10% of the wing span, and its core is located at about $y/b=0.07$ and $x/b=-0.06$, i.e. 7% and 6% of the span above and inward of the wing tip trailing edge, respectively. The helicoidal nature of the vortex and the resultant induced velocities on either side of the vortex core generate a streamwise velocity magnitude distribution that is higher on one side of the vortex core and lower on the other (Figure 3.1 a, left).

Figure 3.1 b shows the measurement results for chordwisely uniform 50 m/s injection. The corresponding momentum coefficient is 0.0767. As it is evident, the injection starts to affect the characteristics of the tip vortex. The size of the vortex gets much bigger occupying an area of about 18-20% of the wing span, i.e. almost two times of its size in the case of no-injection. The injection also pushes the vortex upward and outward, putting its core at about $y/b=0.12$ and $x/b=-0.02$. The turbulence

intensity levels within the vortex core show an increase compared to the no-injection case, consistent with previous studies. The total pressure loss levels are as well higher within the vortex core, and the distributions are consistent with the turbulence intensity variations.

Uniform 60 m/s injection case measurement results are shown in figure 3.1 c. Injection momentum coefficient is 0.1089. As it is seen in the figures the upward and outward motion as well as size of the vortex increases due to an increase in injection speed. The vortex core moves to $y/b=0.14$ and $x/b=0$. It's also interesting to note that the wake region seems to be slightly thicker than the one in the case of 50 m/s uniform injection, and the vortex seems to be separated from the wake zone entraining less amount of wake fluid into the vortex. The low momentum wake zone can also be seen in the velocity magnitude plots as the green contours around the wing trailing edge.

85 m/s chordwise uniform tip injection results are given in Figure 3.1 d. This injection scenario has the highest injection momentum coefficient, i.e. $C_{\mu}=0.2179$. The vortex occupies a larger area compared to lower injection speed scenarios and also seems to entrain much more of the low momentum turbulent wake fluid. The vortex core location has moved outward and upward compared to the lower injection speeds. So the displacement of vortex core is proportional to the injection momentum coefficient, and this is consistent with what has been seen in Heyes and Smith's study[9] for a half span wing model with 150 mm chord and 150 mm half span in a free stream velocity of 22 m/s. Vortex core approximate locations for this study and Heyes and Smith's study is shown in figure 3.2. The corresponding injection momentum coefficient for each case is shown in Table 1.

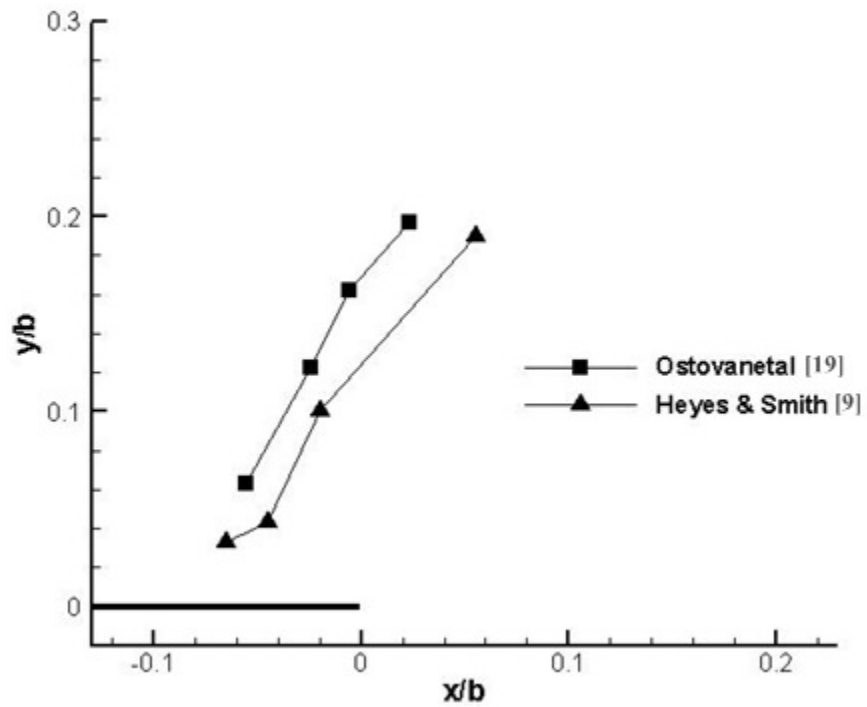


Figure 3.2- Vortex core approximate locations for this study which is represented in Ostovanetal [19] and Heyes and Smith's [9] study. Corresponding injection momentum coefficient for each vortex core location is shown in Table 1

Table 3.1 Injection momentum coefficients for each of vortex core locations shown in figure 3.2

Locations	1	2	3	4
Ostovanetal [19]	No injection	0.002	0.018	0.066
Heyes & Smith [9]	No injection	0.0767	0.1089	0.2179

Turbulence intensity and total pressure loss levels in and around the vortex core for 85 m/s injection speed seem to be reduced compared to the 60 m/s injection speed, so it can lead to the fact that there exists an optimum momentum coefficient. Figure 3.3 shows turbulence intensity and total pressure distributions one chord downstream of the wing along the AA' dashed-lines shown in figure 3.1 for each scenario. AA' dashed-lines are horizontal lines approximately located on tip vortex core of each case. The approximate vortex core locations are obtained using total pressure distribution (minimum total pressure). As it is seen in figure 3.3 uniform injection of 50 m/s has the maximum pressure loss in its vortex core. It is valuable to note that the approximate horizontal location of the vortex core for each scenario is also detectable from the total pressure distribution shown in figure 3.3 right.

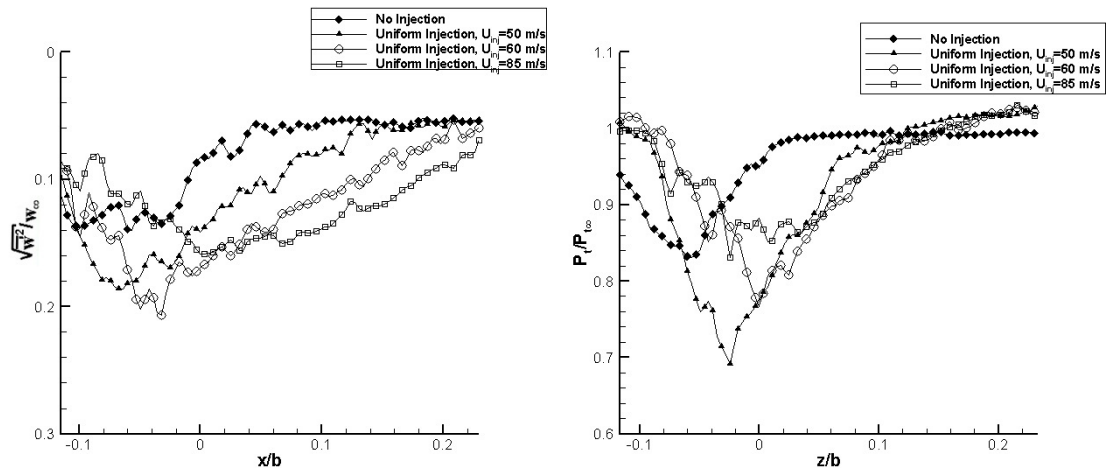


Figure 3.3- Turbulence intensity (left) and total pressure (right) distribution one chord downstream of the wing along the horizontal line intersecting the tip vortex core for three different injection scenarios

3.1.2 Effect of injection velocity with constant C_μ

In this section, the effects of different velocities with constant C_μ in two different injection scenarios are studied. Momentum coefficient for both scenarios is equal to 0.10857. In order to accomplish the same momentum coefficient with varying velocities the first case considered to have 60 m/s chordwisely uniform injection from all of 10 injection holes in the tip and second case is required to have 85 m/s chordwisely uniform injection just from 5 holes (not from every hole but from every other hole). Figure 3.4 shows the streamwise velocity magnitude distribution, turbulence intensity distribution as well as total pressure distribution for both scenarios one chord downstream of the wing.

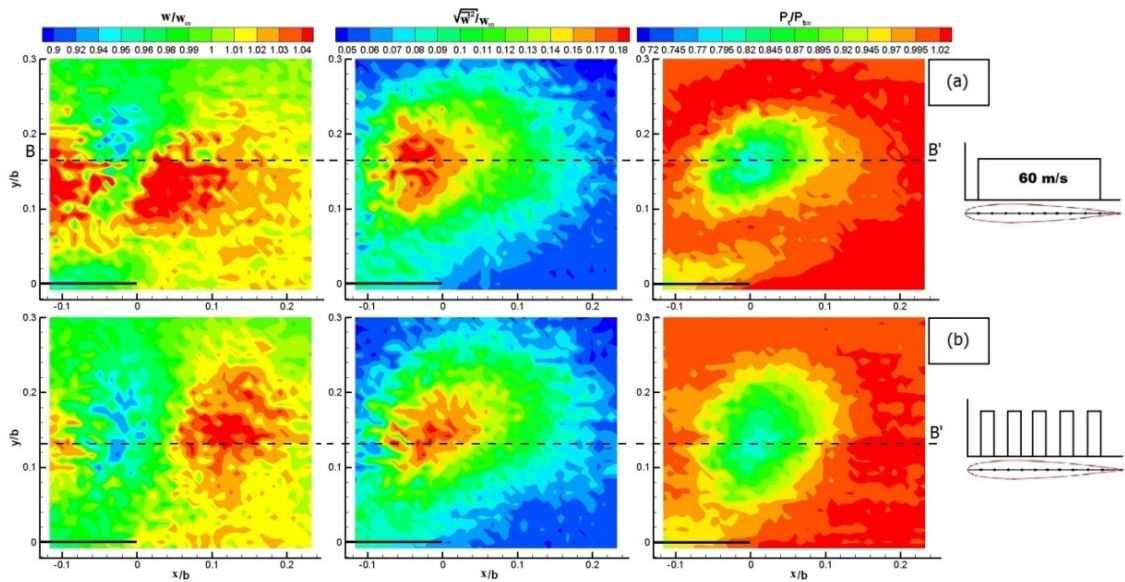


Figure 3.4- The streamwise velocity magnitude (left), turbulence intensity (middle) and total pressure (right) distributions one chord downstream of the wing. (a) 60 m/s uniform (b) 85 m/s uniform (5 hole) injection

Analyzing the figures, a decrease in streamwise velocity magnitude in the vortex region (especially at $0.1 < y/b < 0.2$ and $0 < x/b < 0.1$) is observed when the injection velocity increases. The injection velocity change seems to have no observable effect on turbulence intensity magnitude and its distribution.

In lower injection speed (60 m/s) the vortex and wing's wake interaction is less than 85 m/s case as it's obvious in total pressure distributions in figure 3.4. There is no change in total pressure magnitude of vortex due to injection speed change. But it seems to be an upward motion of the tip vortex core center in 60 m/s injection scenario due to total pressure distribution data. In order to study the effects of different injection speeds with constant momentum injection coefficient, turbulence intensity and total pressure magnitudes along a horizontal line intersecting approximate vortex core of each case is plotted in figure 3.5. The horizontal lines are shown in figure 3.4 as BB' dashed-lines. The vortex core approximate locations are obtained using total pressure distribution (minimum total pressure).

As it is obvious from figure 3.5, the injection speed seems to have no remarkable effects on turbulence intensity and total pressure magnitudes along BB' lines. Although the quantities don't match accurately but the general behavior is the same. So it results that with constant injection momentum coefficient, injection speed variation has no crucial effect on the tip vortex characteristics.

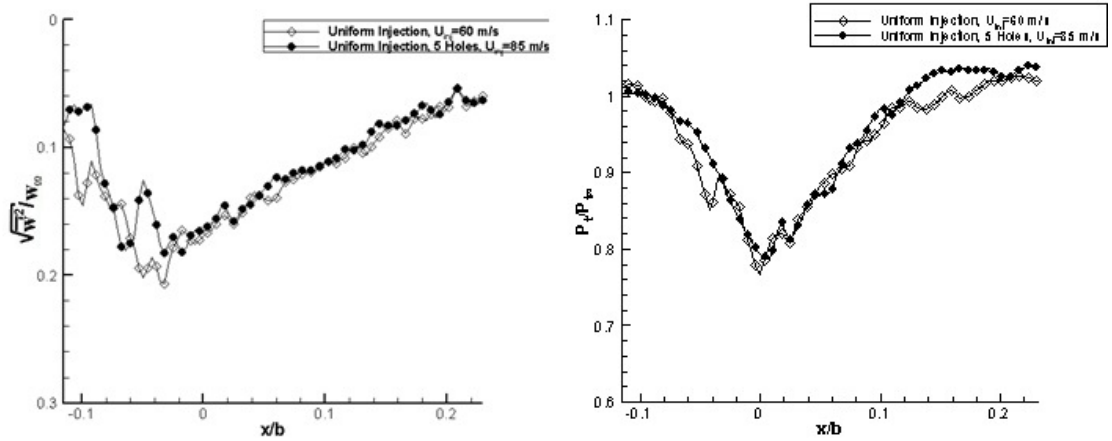


Figure 3.5- Turbulence intensity (left) and total pressure (right) distribution one chord downstream of the wing along the horizontal line intersecting the approximate tip vortex core for two different injection scenarios

3.1.3 Effect of injection waveform with constant C_μ

In this section, the effects of injection waveform with constant injection momentum coefficient on the tip vortex characteristics are studied. Two cases considered for this study. The first case has a constant injection momentum coefficient of 0.075 and consists of three different injection scenarios which are triangular waveform, uniform and reverse triangular waveform. The second case has a constant momentum coefficient of 0.1089 and the injection scenarios are quarter-sine waveform, uniform and reverse quarter-sine waveform. Figure 3.6 shows the injection waveform profiles for two study cases.

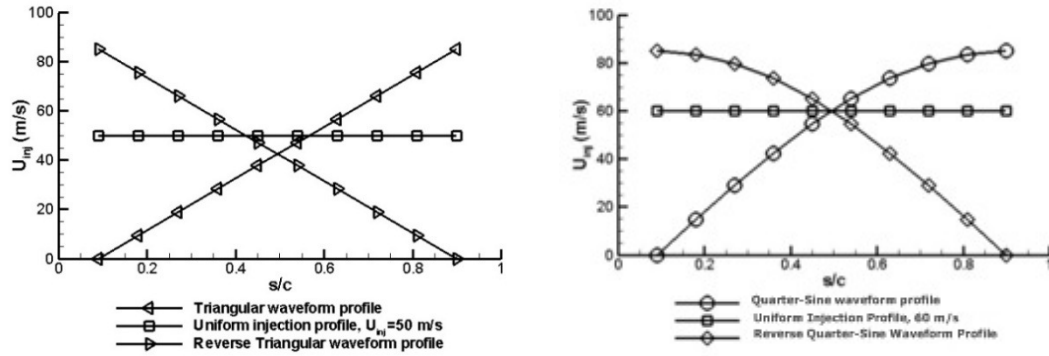


Figure 3.6- Three different injection waveform profiles for 0.075 (right) and 0.1089 (left) injection momentum coefficients

Figure 3.7 shows the streamwise velocity, turbulence intensity as well as total pressure magnitude and distribution one chord downstream of the wing for 3 different injection waveform profiles with constant injection momentum coefficient equal to 0.075. As it is seen in the figure 3.7 different injection waveform profiles have remarkable effects on the tip vortex characteristics. In triangular waveform injection, bigger streamwise velocity magnitudes are seen at $0.1 < y/b < 0.2$ and $0 < x/b < 0.2$ region compared to the uniform and reverse triangular waveform profiles. The vortex size as well as outward and upward motion is also bigger in triangular waveform injection scenario. The pressure loss magnitude in the vortex core is bigger in uniform injection compared to the triangulate waveform injection. The reverse triangular waveform injection has a dissimilar effect on tip vortex compared to other injection scenarios. As it's shown in total pressure distribution the reverse triangular injection spreads the tip vortex in a vertical direction.

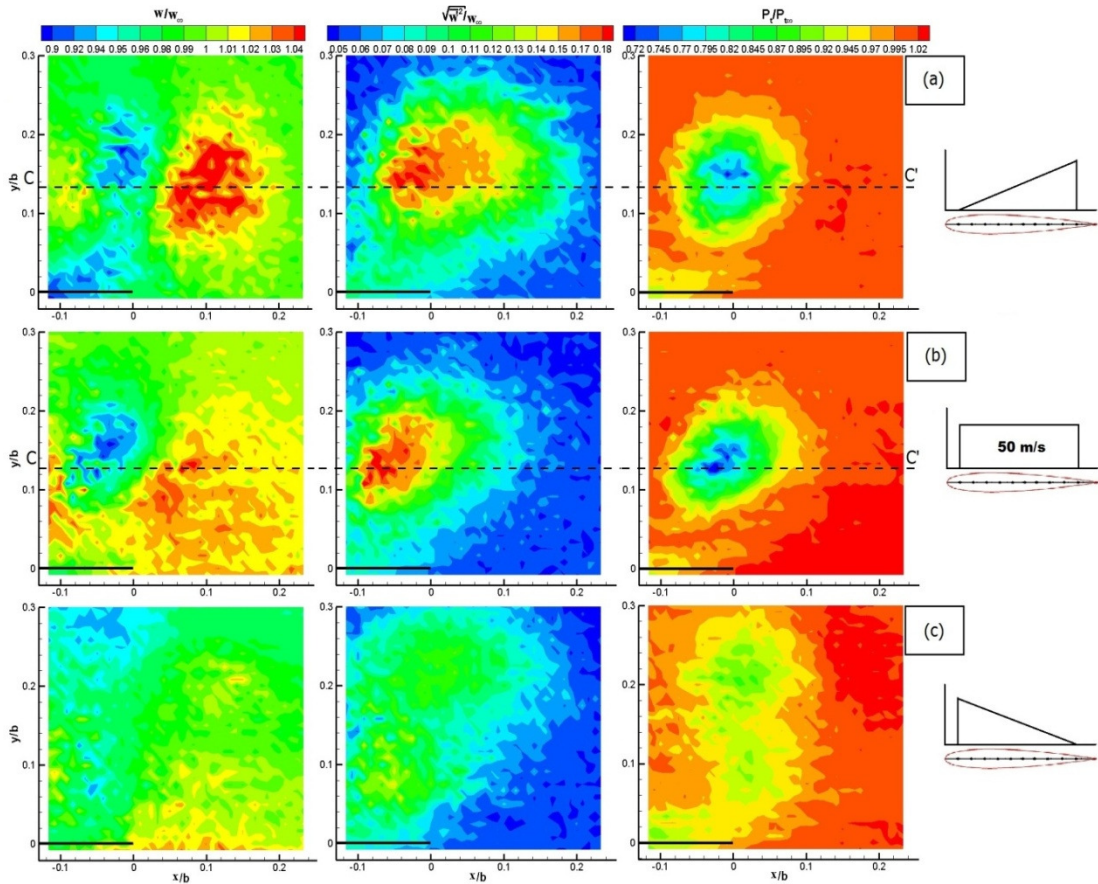


Figure 3.7- The streamwise velocity magnitude (left), turbulence intensity (middle) and total pressure (right) distributions one chord downstream of the wing. (a) triangular waveform injection (b) uniform waveform injection (50 m/s) (c) reverse triangular waveform injection

In order to have a better understanding about the effects of different waveform injections with constant injection momentum coefficient, turbulence intensity and total pressure magnitudes along a horizontal line intersecting vortex core of triangular and uniform injections are plotted in figure 3.8. The horizontal lines are shown in figure 3.8 as CC' dashed-lines. The vortex core locations are obtained using total pressure

distribution (minimum total pressure). As it is obvious from figure 3.8 the vortex core horizontal location differs for two scenarios. There is more outward motion in triangular waveform injection but in the other hand pressure loss magnitude is higher in uniform injection. For turbulence intensity magnitudes there is no notable change.

In second study case the effects of different injection waveforms with constant injection momentum coefficient are studied with a constant momentum coefficient of 0.1089. Measurements are done in three different injection scenarios, quarter-sine waveform injection, 60 m/s uniform injection and reverse quarter-sine waveform injection. The results are shown in figure 3.9. In contrary to what was seen in previous case, An increase in streamwise velocity magnitude is observed for 60 m/s uniform injection at $0 < x/b < 0.1$ and $0 < y/b < 0.1$ region compared to the quarter-sine waveform injection. It can be due to helicoidal nature of the vortex. The tip vortex diameter is also a little bigger in the 60 m/s injection scenario compared to the quarter-sine waveform injection scenario. Turbulence intensity magnitudes in the vortex core are already the same in uniform and quarter-sine waveform injections. A pressure loss magnitude decrease can be seen in 60 m/s uniform injection scenario compared to the quarter-sine injection scenario.

As for reverse triangular injection scenario, reverse quarter-sine injection scenario has also a dissimilar effect on the tip vortex compared to the other injection scenarios. Similar to previous case, in order to have a better understanding about the effect of different waveform injections with constant injection momentum coefficient, turbulence intensity and total pressure magnitudes along a horizontal line intersecting approximate vortex core of quarter-sine and uniform injection scenarios are plotted in figure 3.10. The horizontal lines are shown in figure 3.9 as DD' dashed-lines. The vortex core locations are obtained using total pressure distribution (minimum total pressure)

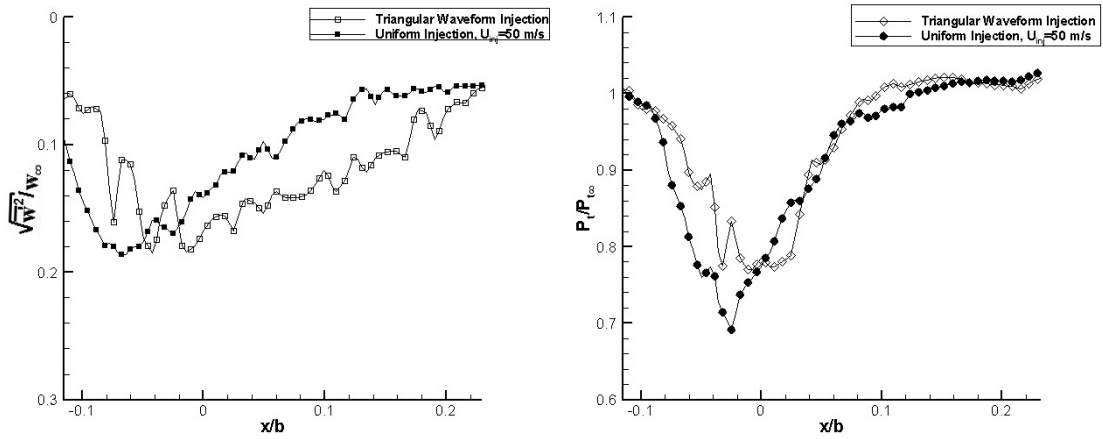


Figure 3.8- Turbulence intensity (left) and total pressure (right) distribution one chord downstream of the wing along the horizontal line intersecting approximate tip vortex core for each different injection scenarios

As it is shown in figure 3.10, there is no significant difference in turbulence intensity magnitudes between 60 m/s uniform and quarter-sine waveform injections but, the pressure loss is bigger for quarter-sine waveform injection scenario. The vortex core coordinates are approximately the same for quarter-sine and 60 m/s uniform injections.

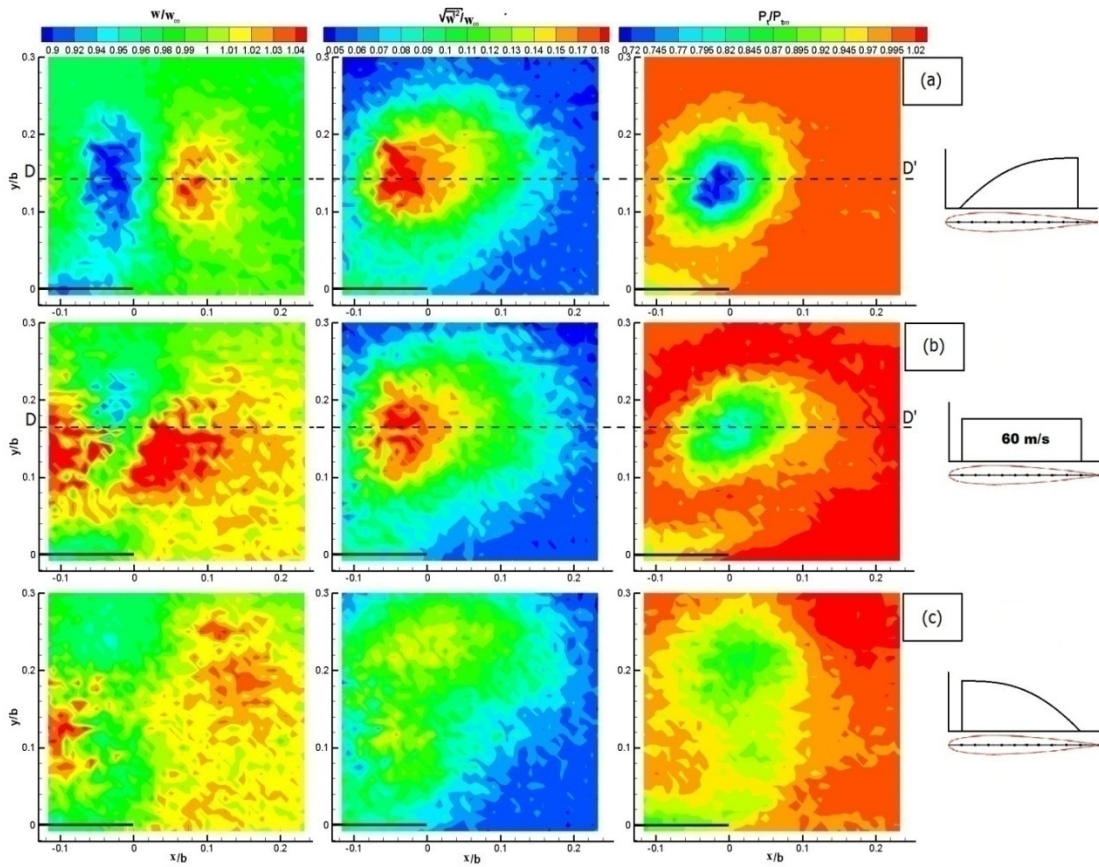


Figure 3.9- The streamwise velocity magnitude (left), Turbulence intensity (middle) and total pressure (right) distributions one chord downstream of the wing. (a) quarter-sine waveform injection (b) uniform injection (60 m/s) (c) reverse quarter-sine waveform injection

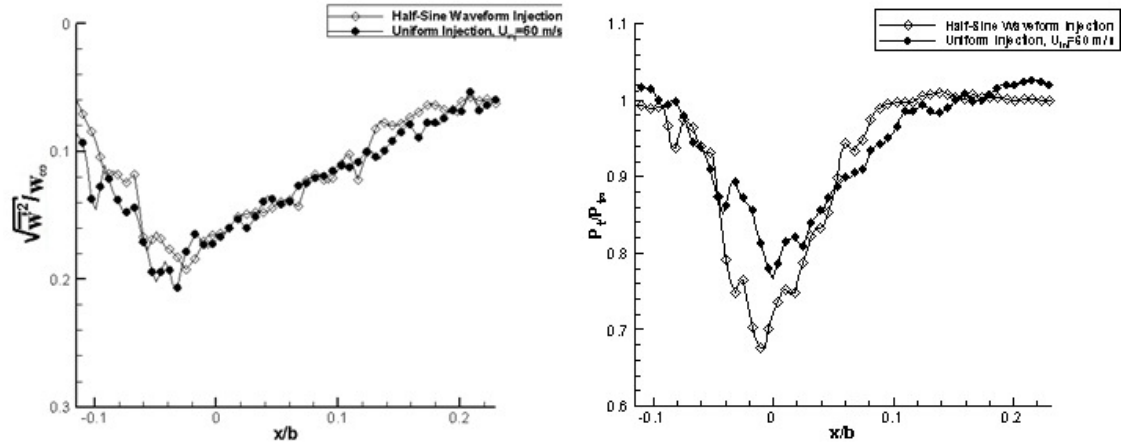


Figure 3.10- Turbulence intensity (left) and total pressure (right) distribution one chord downstream of the wing along the spanwise line intersecting approximate tip vortex core for two different injection scenarios

3.1.4 Effect of tip injection with fixed maximum injection velocity (varying waveforms and C_{μ})

In this section, measurement results for three different injection scenarios are presented and compared to the no injection case. Three of the scenarios involve a steady injection (maximum speed of 85 m/s) from the tip with different geometrical injection patterns, i.e. uniform, triangular and quarter-sine wave injections. The momentum coefficients, C_{μ} , for each one of the injection scenarios are 0.2179, 0.0765 and 0.1089 for the uniform, triangular and quarter-sine injections, respectively. The results are compared to the case with no injection from the wing tip.

Figures 3.11 a, b, c and d present the distributions of streamwise velocity magnitude and turbulence intensity as well as total pressure one chord downstream of

the wing for no-injection, triangular, quarter-sine and uniform injection scenarios, respectively.

In the case of no-injection (Figure 3.11a), the diameter of the vortex is about 10% of the wing span and its core is located at about $y/b=0.07$ and $x/b=-0.06$, i.e. 7% and 6% of the span above and inward of the wing tip trailing edge, respectively. The helicoidal nature of the vortex and the resultant induced velocities on either side of the vortex core generate a streamwise velocity magnitude distribution that is higher on one side of the vortex core and lower on the other (Figure 3.11a, left). The wake of the wing is also visible as a low total pressure high turbulence zone that is aligned quite well with the trailing edge of the wing.

Figure 3.11b shows the measurement results for triangular injection. The corresponding momentum coefficient is 0.0767. As is evident, the injection starts to have an effect on the characteristics of the tip vortex. The size of the vortex gets much bigger occupying an area of about 18-20% of the wing span, i.e. almost two times of its size in the case of no-injection. The injection also pushes the vortex upward and outward, putting its core at about $y/b=0.15$ and $x/b=0$. The turbulence intensity levels within the vortex core shows an increase compared to the no-injection case, consistent with previous studies. The total pressure loss levels are also higher within the vortex core and the distributions are consistent with the turbulence intensity variations. It's also interesting to note that the wake region seems to be slightly thicker than the one in the case of no-injection and the vortex seems to be separated from the wake zone entraining less amount of wake fluid into the vortex. The low momentum wake zone can also be seen in the velocity magnitude plots as the blue contours around the wing trailing edge.

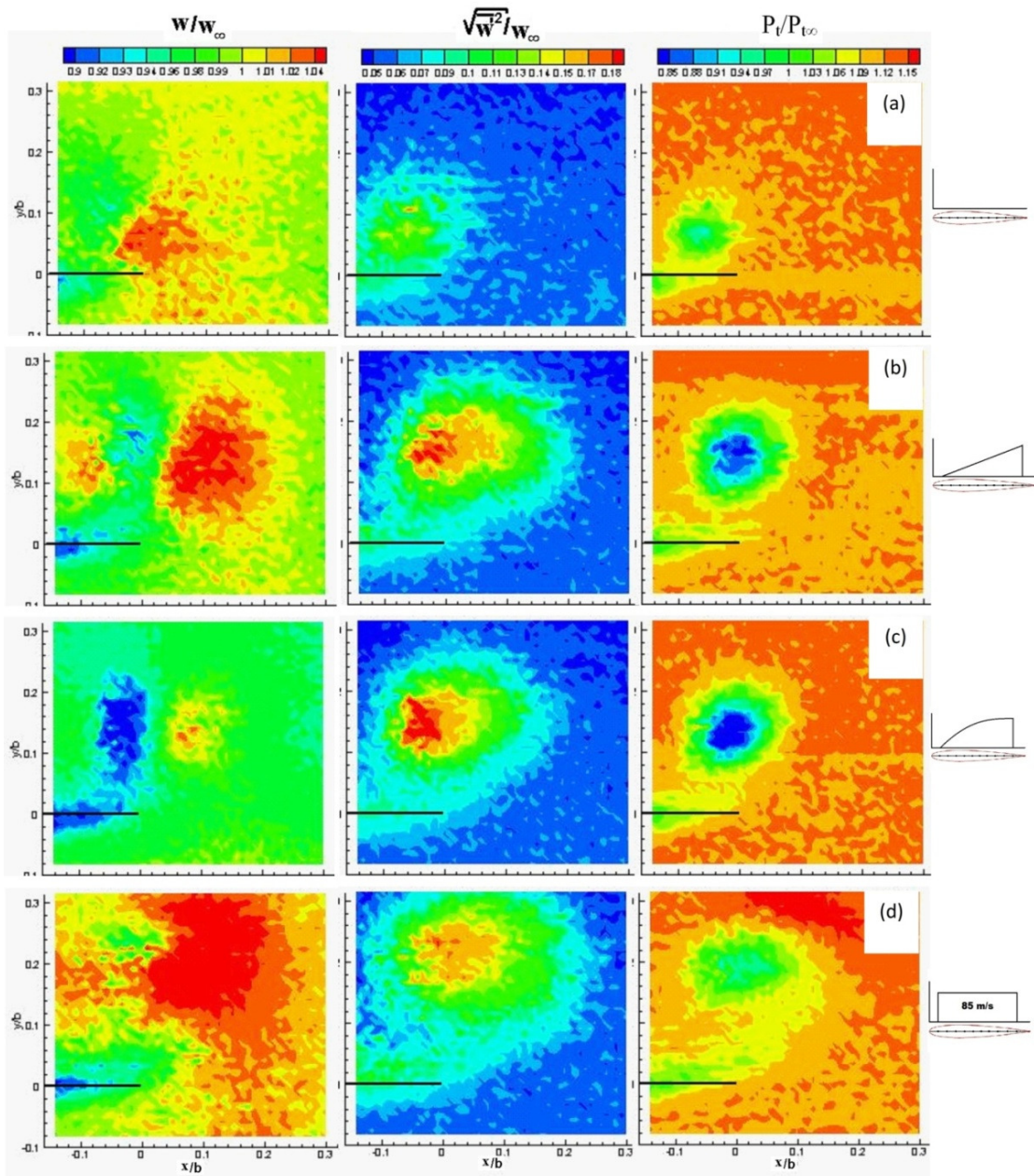


Figure 3.11- The streamwise velocity magnitude (left), turbulence intensity (middle) and total pressure (right) distributions one chord downstream of the wing. (a) no injection (b) steady triangular (c) steady quarter-sine and (d) steady uniform injections. The maximum tip injection velocity for all scenarios is 85 m/s

The results of the steady quarter-sine injection are presented in Figure 3.11c. When compared to the triangular injection, the size of the vortex seems to get slightly smaller and the vortex core gets slightly shifted inwards. The turbulence intensity and the total pressure loss levels within the vortex core are higher compared to those in the case of triangular injection. The mean streamwise velocity field seems to be affected significantly. The low momentum region on one side of the vortex (blue contours extending from $y/b=0.05$ to 0.21 at $x/b=-0.02$) seems to be greatly enhanced. This suggests a possible change in the helicoidal geometry of the vortex.

Full chordwisely uniform tip injection results are given in Figure 3.11d. This scenario has the highest injection momentum coefficient, i.e. $C_{\mu}=0.2179$. The vortex occupies a larger area compared to triangular and quarter-sine scenarios and also seems to entrain much more of the low momentum turbulent wake fluid. However, the turbulence intensity and total pressure loss levels in and around the vortex core seems to be reduced compared to the other injection scenarios.

3.1.5 Effect of tip injection on total pressure loss

Figure 3.12 shows total pressure distributions one chord downstream of the wing. Black lines indicate the wing trailing edge and (0,0) coordinate is the trailing edge of the wing tip. The maximum tip injection velocity for all scenarios is 85 m/s. As it is seen in the figure total pressure distribution for reverse triangular and reverse quarter-sine wave from injections gets a completely different structure compared to the other injection scenarios. Figure 3.13 is presented to examine the results of all scenarios in terms of total pressure magnitudes in the approximate vortex core location of each scenario. The corresponding injection momentum coefficient for each scenario is shown on horizontal axis. As it is detectable from figure 20 there exists an optimum tip injection coefficient for maximum pressure loss in the approximate vortex core

location. It is interesting that the total pressure magnitude of approximate vortex core location for 85 m/s uniform injection scenario is bigger than the one for no injection scenario, so we can conclude that after some point, the increase of the C_{μ} starts to have a decreasing effect on the pressure loss of the tip vortex core.

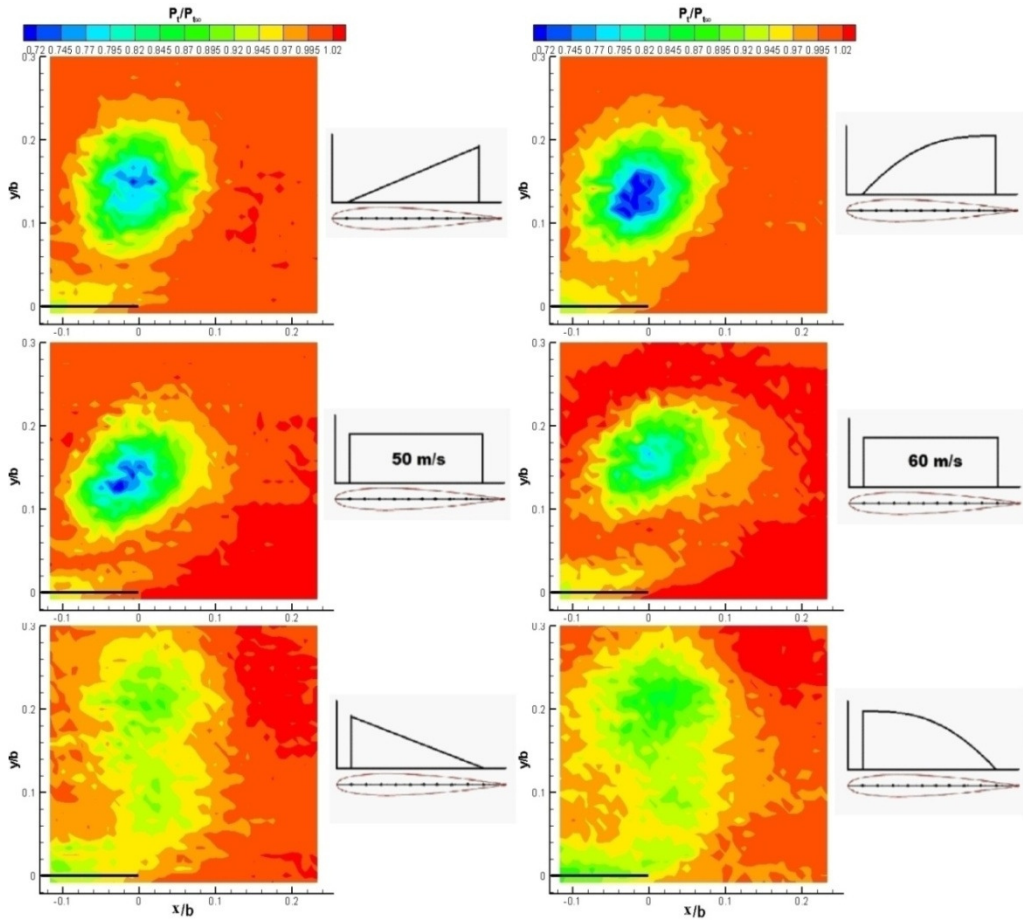


Figure 3.12- Total pressure distributions one chord downstream of the wing. The maximum tip injection velocity for all scenarios is 85 m/s

Table 3.2 presents area averaged total pressure calculations minus atmospheric pressure for no injection, triangular injection, quarter-sine injection and uniform injection with a maximum injection velocity of 85 m/s. The maximum pressure loss belongs to quarter-sine injection scenario which is consistent with the results shown in figure 3.13 as in quarter-sine injection scenario total pressure of approximate vortex core location has the minimum value compared to other injection scenarios.

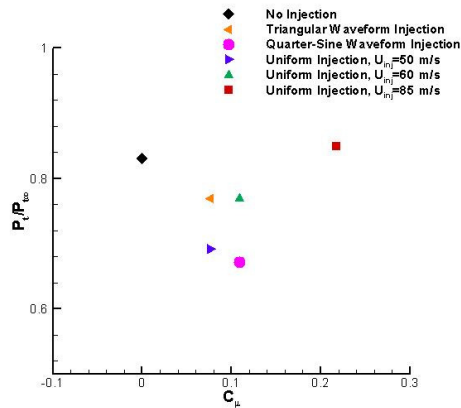


Figure 3.13- Total pressure magnitudes in the approximate vortex center location of each scenario. Corresponding injection momentum coefficient for each scenario is shown on horizontal axis

Table 3.2 Area averaged total pressure minus atmospheric pressure calculations for no injection, triangular injection, quarter-sine injection and uniform injection with a maximum injection velocity of 85 m/s

Injection Scenario	$P_t - P_a$ (Pa)
No Injection	101,649272
Triangular Injection	101,776349
Quarter-Sine Injection	101,214908
Uniform Injection	102,215532

3.2 Stereoscopic PIV measurement results

Figure 3.14 shows the total pressure, mean in-plane velocity magnitude with superimposed in-plane streamlines and the mean vorticity magnitude distributions one chord downstream of the wing trailing edge for triangular, quarter-sine and uniform injection patterns as well as for the case where there is no injection from the wing tip. These cases all involve steady injection from the tip and for all cases the maximum injection velocity, which is about 85 m/s, is kept fixed. The corresponding chord-averaged momentum coefficients, C_{μ} , for the triangular, quarter-sine and uniform injections are 0.0765, 0.1089 and 0.2179, respectively. Keep in mind that the velocity and vorticity data are averages of 140 instantaneous vector maps after vortex meandering effects are removed. The black line in the figure represents the trailing edge of the wing and the $(x,y)=(0,0)$ coordinate is the corner of the trailing edge and the wing tip. As can be seen in the figure, available measurement areas are all different for each scenario mainly due to the fact that the common overlap areas are different for each injection case after meandering effects are removed, as described previously.

As is evident for all cases, the region occupied by the tip vortex is characterized in general by low total pressure, swirling streamlines and concentrated positive vorticity. In Figures 3.14b, c and d several effects of injection on the tip vortex can readily be observed:

- 1) Vortex core relocation: In the case of no-injection (Figure 3.14a), the vortex core is located at about $x/b=-0.05$ $y/b=0.06$, i.e. the vortex center is about 5% of the span inwards from the wing tip and about 6% span above the wing trailing edge. For the triangular injection (Figure 3.14b), the vortex center is now located at about 2.5% of the span away from the tip in the spanwise direction (outwards) and 14% of the span above the trailing

edge. Compared to the no-injection case the vortex has moved considerably away from the wing tip. The quarter-sine injection (Figure 3.14c) pushes the vortex more or less to the same position as that in the case of triangular injection in spite of the fact that the average momentum coefficient is about 30% higher for the quarter-sine injection. In the case of uniform injection (Figure 3.14d) where the average momentum coefficient is almost three times higher the vortex is further pushed outward to 6% span away from the tip and to 18% span up from the trailing edge of the wing.

- 2) Vortex size enlargement and shape distortion: When there is no injection, the shape of the tip vortex is quite symmetrical and its diameter is about 6% of the wing span as can be seen from the vorticity plots in Figure 3.14. Both the triangular and the quarter-sine injection patterns distort the shape of the vortex, stretching it especially along the y-coordinate while the size of the vortex in the spanwise direction keeps more or less unchanged. The dimension of the vortex in y-direction is about 15% of the span for the triangular injection and slightly larger for quarter-sine injection. When the injection is performed uniformly, the symmetry of the vortex gets re-established but now the vortex is much larger occupying a region that has a diameter about 16% of the wing span.

- 3) Secondary vortex formation: In all injection cases, a secondary vortex structure with opposite sense of rotation and with a much lower vorticity magnitude is observed right next to the tip vortex. This vortex is visible as the blue contour regions in the vorticity plots of Figures 3.14b and c and it is mostly out of the field of view in Figure 3.14d though it still exists. The created by a free-jet flow issuing in to a still ambient. The side vortex with the negative sign remains in the flow field and the one with the positive

sign possibly gets entrained in to the tip vortex. Similar vortices are also observed by other researchers (Margaris and Gursul [7] saw a pair of counter rotating vortices attached to the jet exit at $x/c=-0.75$).

- 4) Variations in total pressure loss levels: The total pressure distributions measured by the Kiel probe and presented in Figure 3.14 are very much consistent with the velocity and vorticity distributions measured by the PIV system. The regions occupied by the tip vortex have reduced total pressure levels compared to the surroundings. As the vortex size gets larger due to tip injection, the size of the region with low total pressure also increases as expected. However, the level of total pressure loss does not seem to increase in parallel with increasing momentum coefficient. The core of the vortex in quarter-sine injection has the maximum reduction in total pressure compared to the other cases.

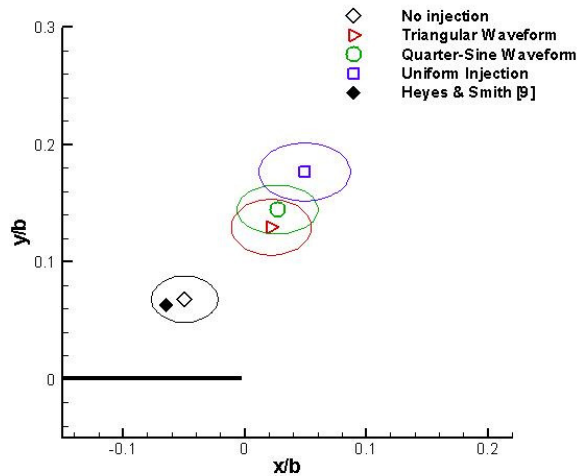


Figure 3.15- Mean vortex center locations with respect to the wing ($x/b=0$ is the same as defined in Figure 3.14). The ellipses show the degree of meandering around each vortex center such that the r_x and r_y radii are the root-mean-square values of vortex center position fluctuation around the mean

Effects of uniform and waveform injection are investigated also on the flow around the vortex core center. Keep in mind that the location of the vortex center changes instantaneously due to the meandering of the tip vortex and we determine the center position in each available instantaneous vector map based on the positive maximum vorticity location. These values are then used to calculate the mean value of the vortex center position. Figure 3.15 presents the mean center locations for each injection scenario with respect to the wing. The ellipses around each mean vortex center are indicators of the degree of meandering such that r_x and r_y radii of the ellipses are the root-mean-squares of the instantaneous center location fluctuations around the mean. As can be seen the meandering ranges are close for each injection case with the no-injection and the uniform injection cases having the smallest and the largest compared to the others. The no-injection case is also compared to the vortex position

measured by Heyes and Smith [9] for a half span wing model with 150 mm chord and 150 mm half span in a free stream velocity of 22 m/s, which seems to be in agreement with the current measurement and within the range of vortex meandering.

Figures 3.16a and 3.16b show the re-centered vorticity distributions and the tangential velocity components around mean vortex centers for all injection scenarios (i.e. the $x'=0$ coordinate is the mean vortex center). The maximum level of vorticity at the center of the vortex seems to be reduced for the triangular and quarter-sine injections compared to the no-injection case. The uniform injection is as high as the no-injection case but distributed in a wider area around the center. The negative values after $x'/b=0.05$ are due to the effect of the secondary vortex discussed previously.

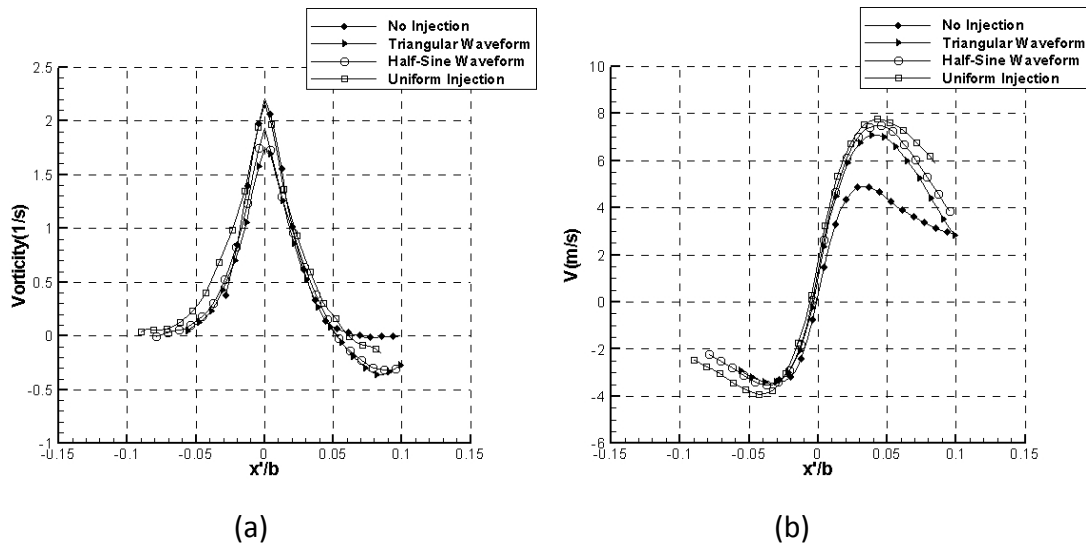


Figure 3.16- (a) Mean vorticity and (b) tangential velocity distributions around the mean vortex centers

Figure 3.17 shows Normal stress components' distributions one chord downstream of the wing trailing edge. Black line represents the trailing edge of the wing and the $(x,y)=(0,0)$ coordinate is the corner of the trailing edge and the wing tip. $b=0.3$ m is the wing span. For each injection scenario, mean center location and meandering range are shown as circle and ellipse around, respectively. As it is evident, in triangular injection case, there are higher levels of normal stress components in the vortex region compared to no injection case. By increasing the injection momentum coefficient from triangular to uniform injection cases, normal stress components' levels also increase in the tip vortex region. Figure 3.18 shows shear stress components' distributions one chord downstream of the wing trailing edge. Black line represents the trailing edge of the wing and the $(x,y)=(0,0)$ coordinate is the corner of the trailing edge and the wing tip. $b=0.3$ m is the wing span. In each plot, mean center location of the tip vortex and meandering range are shown as circle and ellipse around, respectively. As it is obvious, by increasing the injection momentum coefficient the shear stress components' magnitudes also increase. The next notable fact is that the shear stress components have a higher magnitude not at vortex center mean location but around them.

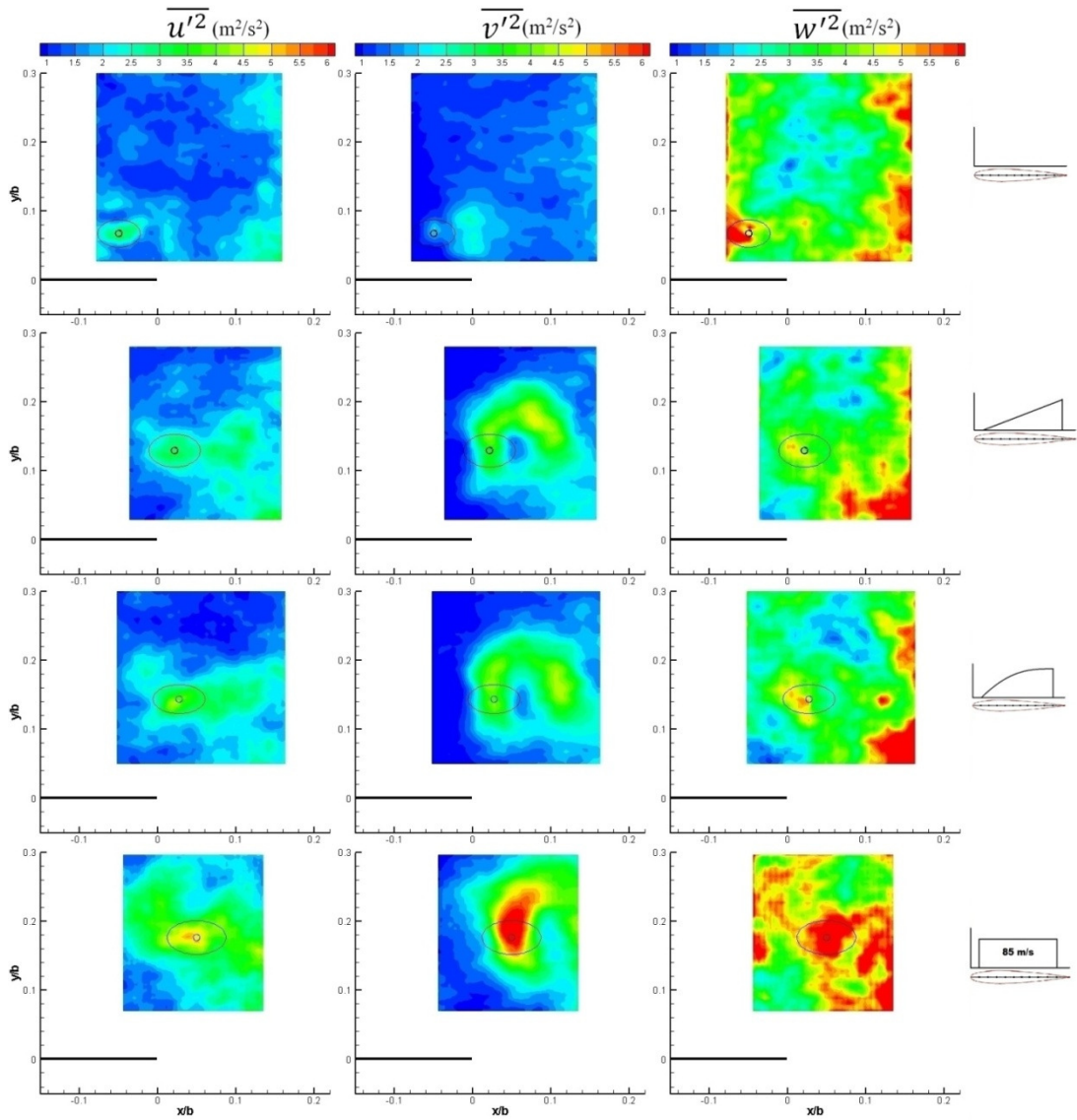


Figure 3.17- Normal stress components' distributions one chord downstream of the wing trailing edge. Black line represents the trailing edge of the wing and the $(x,y)=(0,0)$ coordinate is the corner of the trailing edge and the wing tip

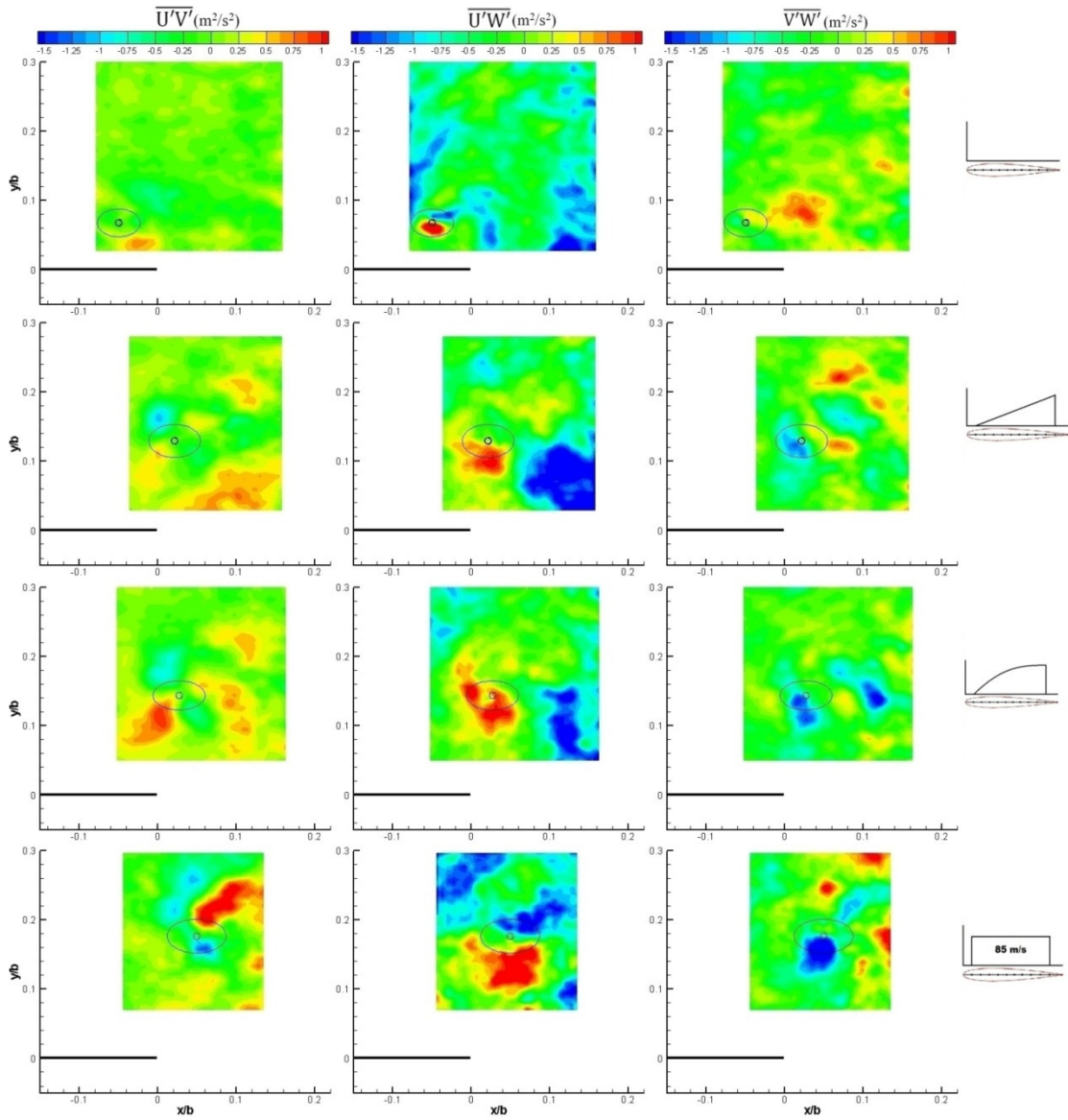


Figure 3.18- Shear stress components' distributions one chord downstream of the wing trailing edge. Black line represents the trailing edge of the wing and the $(x,y)=(0,0)$ coordinate is the corner of the trailing edge and the wing tip

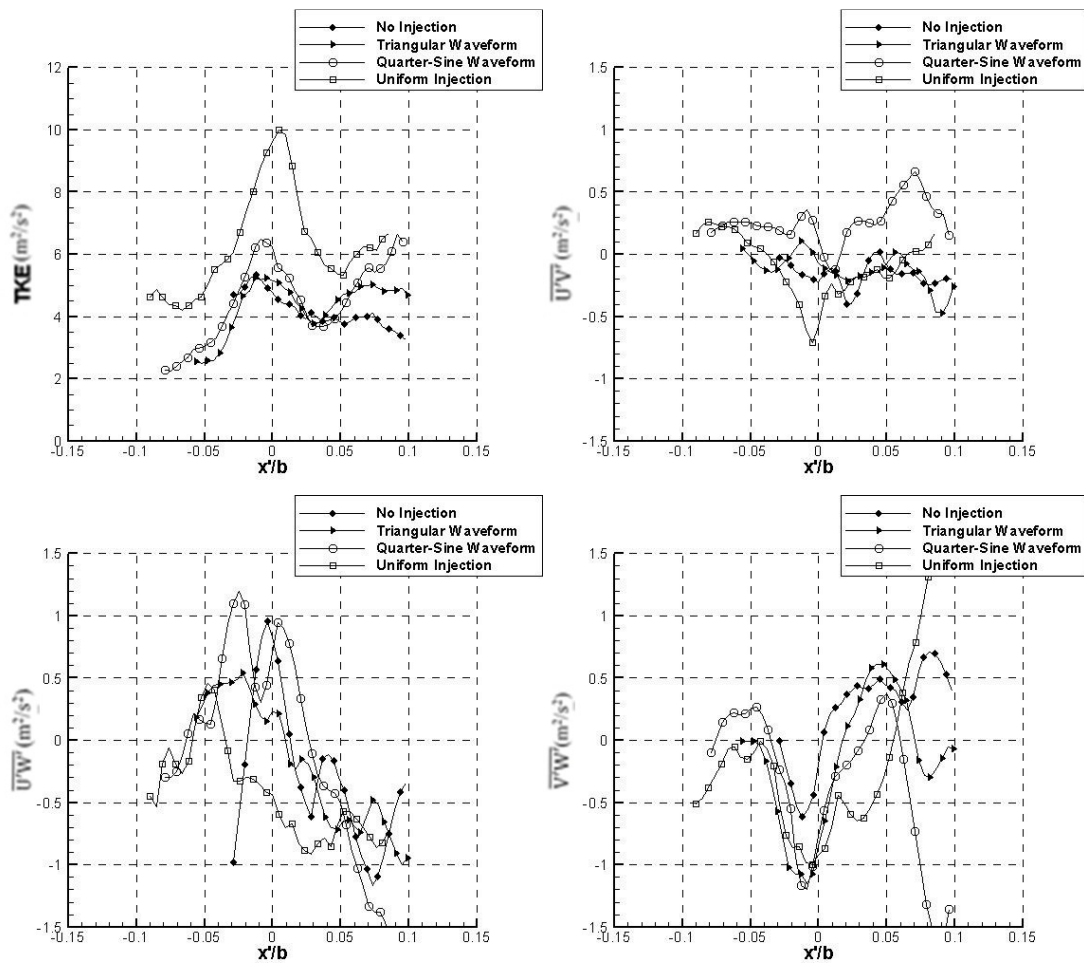


Figure 3.19- Turbulent kinetic energy and shear stress components distributions around the mean vortex centers for four different injection scenarios

Figure 3.19 shows turbulent kinetic energy and shear stress components distributions around the mean vortex centers related to four different injection scenarios. As it is obvious in turbulent kinetic energy distribution, for all scenarios, it has a maximum value somewhere around the mean vortex center. The other notable point is the increasing of turbulent kinetic energy at the mean vortex center area by increasing the injection momentum coefficient. The growing of values after $x'/b=0.05$ are due to the effect of the secondary vortex discussed previously. In shear stress

components' distributions around the mean vortex centers, by increasing the injection momentum coefficient higher levels of shear stress components are depicted around the mean vortex center locations.

3.3 Energy budget calculations

In this section, consumed power for injection in each injection scenario is examined being related to the corresponding circulation magnitude changed due to the injection. Power consumption and corresponding circulation magnitudes for four injection scenarios are given in Table 3.3. All scenarios have the maximum injection speed of 85 m/s. As it is evident from shown data, in uniform injection case an energy consumption of 17 watts leads to an increase in circulation for about two times. From aerodynamic principles, it is known that circulation has a direct relation with the wing's lift force. So by increased circulation the lift force of the wing is expected to increase.

Table 3.3. Injection momentum coefficient, Power consumption and corresponding circulation magnitudes for four injection scenarios

Injection Scenario	C_{μ}	Energy Consumption (W)	Circulation
No Injection	0	0	0.013270879
Triangular	0.07667	4.726720534	0.024204567
Quarter-Sine Injection	0.1086	7.3503364	0.01821819
Uniform Injection	0.2179	17.01619392	0.028932873

CHAPTER 4

CONCLUSIONS

Experimental results are presented on the effect of chordwise modulated tip injection with different injection momentum coefficients from the wing tip of a rectangular wing with an aspect ratio of three. Mean flow, turbulence and total pressure loss characteristics in and around the tip vortex are presented one chord downstream of the wing trailing edge for chordwise uniform, triangular, reverse triangular, half-sine and reverse half-sine injection patterns utilizing single sensor hotwire and Kiel probe measurement techniques. Furthermore, Stereoscopic PIV measurements are also done one chord downstream of the wing and flow field 3D velocity components are measured.

Current data show consistent trends with previously observed effects of steady uniform tip injection such as the upward and outward motion of the vortex as well as increased levels of turbulence intensity and pressure loss within the vortex core. The vortex size gets bigger with injection, and the total pressure levels get reduced significantly near the vortex core. The injection pattern also seems to affect the size of the wing wake as well as the wake entrainment characteristics of the tip vortex. Depending on the injection waveform pattern the helicoidal shape of the tip vortex also seems to get affected. The injection momentum coefficient has also a significant effect on tip vortex characteristics. By increasing C_{μ} , turbulence intensity and pressure loss magnitudes of vortex core center increase up to an optimum value of C_{μ} . For injection

momentum coefficients bigger than that optimum value the bigger C_{μ} results in smaller pressure loss and turbulence intensity magnitudes. In this study, Quarter-sine waveform injection is observed to have the maximum effect on pressure loss for most of the injection momentum coefficient magnitudes. As a result of this study it is experienced that the effects of vortex meandering on tip vortex characteristics are very important in studying vortices, and those effects needs to be filtered from the measured data.

Future work in order to improve this study, can focus on three different topics, which are,

- 1- Repeating the experiments for the same conditions studied in this work to check the consistency and repeatability.
- 2- Doing the measurement for different conditions than studied here, such as changing the waveforms, injection momentum coefficient, Different Reynolds numbers and etc.
- 3- Investigating the effect of tip injection on the wings lift and drag force. This work can be performed by connecting the isolated wing model to a balance system to measure aerodynamic moment and forces.

REFERENCES

- [1] Gerontakos, P., Lee, T., “Near-field tip vortex behind a swept wing model”, *Experiments in Fluids*, 40 (1), pp. 141-155, 2006.
- [2] Birch, D., Lee, T., Mokhtarian, F., Kafyeke, F., “Structure and Induced Drag of a Tip Vortex”, *Journal of Aircraft*, Vol. 41, No. 5, September–October 2004.
- [3] Gursul, I., Vardaki, E., Margaris, P., Wang, Z., “Control of Wing Vortices”, *Active Flow Control, Notes on Numerical Fluid Mechanics and Multidisciplinary Design*, pp.137-151, Springer-Verlag Berlin, 2007.
- [4] Matalanis, C. G., Nelson, G. D., Eaton, J. K., 2007, “Novel Aerodynamic Device for Wake Vortex Alleviation,” *AIAA Journal*, Vol. 45, No. 9.
- [5] Panagakos, A., Lee, T., 2006, “Tip Vortex Control via an Active Trailing Edge Tab,” *Journal of Aircraft*, Vol. 43, No.4.
- [6] Greenblatt, D., Pack-Melton, L. G., Yao, C. S., Harris, J., 2005, “Active Control of a Wing Tip Vortex,” AIAA 2005-4851. 23rd AIAA Applied Aerodynamics Conference, 6-9 June 2005, Toronto, Canada.
- [7] Margaris, P., Gursul, I., 2004, “Effect of Steady Blowing on Wing Tip Flow Field,” AIAA 2004-2619. 2nd Flow Control Conference, Portland, Oregon, June-July 2004.

- [8] Bettle, J. R., "Experimental Study of a Wing Tip Vortex With Tip Blowing", M.Sc. Thesis, The University of New Brunswick, Canada, Oct. 2004.
- [9] Heyes, A. L., Smith, D. A. R., "Spatial Perturbation of a Wing Tip Vortex Using Pulsed Spanwise Jets," *Experiments in Fluids*, Vol.37, 2004, pp. 120-127.
- [10] Tavella, D. A., Wood, N. J., Lee, C. S., Roberts, L., "Lift Modulation with Lateral Wing-Tip Blowing," *Journal of Aircraft*, Vol. 25, No. 4, 1988.
- [11] Karthikeyan, D., Baeder, J. D., "Control of Rotor Tip Vortex Structure Using Blowing Devices," *American Helicopter Society, 60th Annual Forum Proceedings*, pp. 1952-1967, 2004.
- [12] Karthikeyan, D., Baeder, J. D., "Numerical Simulation of the Effect of Spanwise Blowing on Tip Vortex Formation," *Journal of Aircraft*, Vol. 43, No 4, 2006.
- [13] Coton, F. N., Green, R. B., Early, J. M., Price, J. L., "Amelioration of Blade Vortex Interaction Using Blade Tip Jets," *American Helicopter Society, 61st Annual Forum Proceedings*, pp. 1874-1885, 2005.
- [14] Vasilescu, R., Dancila, D. S., "Modeling of Piezoelectrically Modulated and Vectored Blowing for a Wing Section," *AIAA 2003-219, 41st AIAA Aerospace Sciences Meeting and Exhibit, 6-9 January 2003, Reno, Nevada, 2003.*
- [15] Margaris, P., Gursul, I., "Wing Tip Vortex Control Using Synthetic Jets," *Aeronautical Journal*, Vol. 110., No. 1112, pp. 673-681, 2006.

- [16] Schönfeld, T., Boussuge, J.-F., Le Dizès, S., Leweke, T., “Fundamental Vortex Phenomena: Instabilities And Interactions With Jets And Wakes”, http://www.cerfacs.fr/~cfdbib/repository/TR_CFD_07_78.pdf, (last accessed date: 5th september 2011)
- [17] Westerweel, Scarano, “Universal Outlier Detection for PIV Data”, *Experiments in Fluids* 39, pp 1096-1100, 2005.
- [18] Leweke, T., Roy C., “Experimental Study of Vortex Meandering”, 17th Australasian Fluid Mechanics Conference, 5-9 December 2010, Auckland, New Zealand.
- [19] Ostovan, Y., Mercan, B., Dogan, E., Uzol, O., “Aktif Uç Enjeksiyonunun Kanat Uç Girdabı Yapısı Üzerindeki Etkilerinin Deneysel İncelenmesi”, 3rd National Aerospace Conference, 16-18 September 2010, Anadolu University, Eskisehir, Turkey.
- [20] Pino C. D., Anguita L. P., Alonso J. M. L., Felli M., Ortega S. P., Fernandez-Feria R. “Experimental Measurements Of Wing Tip Trailing Vortices Through Piv And Their Comparison With Theoretical Models” Technical Report Of The Project P05-Tep-170, Universidad de M´alaga, June 16, 2010.
- [21] S. C. C. Bailey and S. Tavoularis. Measurements of the velocity field of a wing-tip vortex, wandering in grid turbulence. *J. Fluid Mech.*, 601:281–315, 2008
- [22] Airfoil Investigation Database, <http://www.worldofkrauss.com/foils/1714>, (Last accessed date: 5th October 2011)